

## CERKL, a retinal dystrophy gene, regulates mitochondrial function and dynamics in the mammalian retina

Serena Mirra<sup>a,b,c,\*</sup>, Rocío García-Arroyo<sup>a</sup>, Elena B. Domènech<sup>a,b</sup>, Aleix Gavaldà-Navarro<sup>c,d,e</sup>, Carlos Herrera-Úbeda<sup>a</sup>, Clara Oliva<sup>f</sup>, Jordi Garcia-Fernàndez<sup>a</sup>, Rafael Artuch<sup>b,f</sup>, Francesc Villarroya<sup>c,d,e</sup>, Gemma Marfany<sup>a,b,c,\*</sup>

<sup>a</sup> Department of Genetics, Microbiology and Statistics and Institute of Biomedicine (IBUB), Faculty of Biology, University of Barcelona, Barcelona, Spain

<sup>b</sup> Centro de Investigación Biomédica en Red de Enfermedades Raras (CIBERER), Instituto de Salud Carlos III, Barcelona, Spain

<sup>c</sup> Institut de Biomedicina de la Universitat de Barcelona- Institut de Recerca Hospital Sant Joan de Déu, IBUB-IRSJD, Barcelona, Spain

<sup>d</sup> Department of Biochemistry and Molecular Biomedicine, Barcelona, Spain

<sup>e</sup> CIBEROBN, Instituto de Salud Carlos III, Spain

<sup>f</sup> Clinical Biochemistry Department, Hospital Sant Joan de Déu, Spain

### ARTICLE INFO

#### Keywords:

Retinal dystrophies  
Retinitis pigmentosa  
CERKL  
Mitochondrial dysfunction

### ABSTRACT

The retina is a highly active metabolic organ that displays a particular vulnerability to genetic and environmental factors causing stress and homeostatic imbalance. Mitochondria constitute a bioenergetic hub that coordinates stress response and cellular homeostasis, therefore structural and functional regulation of the mitochondrial dynamic network is essential for the mammalian retina. *CERKL* (ceramide kinase like) is a retinal degeneration gene whose mutations cause Retinitis Pigmentosa in humans, a visual disorder characterized by photoreceptors neurodegeneration and progressive vision loss. *CERKL* produces multiple isoforms with a dynamic subcellular localization. Here we show that a pool of *CERKL* isoforms localizes at mitochondria in mouse retinal ganglion cells. The depletion of *CERKL* levels in *Cerkl*<sup>KD/KO</sup> (knockdown/knockout) mouse retinas cause increase of autophagy, mitochondrial fragmentation, alteration of mitochondrial distribution, and dysfunction of mitochondrial-dependent bioenergetics and metabolism. Our results support *CERKL* as a regulator of autophagy and mitochondrial biology in the mammalian retina.

### 1. Introduction

Autophagy is an intracellular catabolic pathway where damaged organelles, toxic aggregates or cell components are engulfed and delivered to lysosomes for degradation and recycling, to produce energy and nutrients that are necessary to maintain metabolic homeostasis, particularly in conditions such as starvation or cellular stress (Boya et al., 2013). Autophagy is finely regulated at the molecular level through a set of Atg proteins, such as Beclin 1, which contribute to the initiation and elongation of autophagosomes, and more downstream factors, such as LC3 or p62 (Gatica et al., 2018). Selective autophagy of

mitochondria, known as mitophagy, represents an important mechanism for organelle quality control. Mitochondria are very dynamic organelles that can fuse and divide, move throughout the cell and undergo regulated turnover through mitophagy (Mandal and Drerup, 2019). They can readily adapt to changes in cellular requirements after physiological or environmental cues. When cells are subjected to mild stresses such as nutrient deprivation, mitochondria fuse and form a branched and interconnected network, as a means to increase ATP production and recover cellular homeostasis. Conversely, in the case of severe stress, mitochondria are fragmented to facilitate mitophagy (Zemirli et al., 2018). Defects in general autophagy, mitophagy and mitochondrial

**Abbreviations:** IRDs, Inherited Retinal Dystrophies; RP, Retinitis Pigmentosa; CERKL, CERamide Kinase Like; CRD, Cone-Rod Dystrophy; DAGK, diacylglycerol kinase domain; PH, Pleckstrin homology; RGCs, retinal ganglion cells; DIV, days in vitro; HCQ, hydroxychloroquine; AR, Aspect Ratio; FF, Form factor; RPE, retinal pigment epithelium; OXPHOS, oxidative phosphorylation system; ATP, adenosine triphosphate; OCR, oxygen consumption rates; ECAR, extracellular acidification rates.

\* Corresponding authors at: Department of Genetics, Microbiology and Statistics and Institute of Biomedicine (IBUB), Faculty of Biology, University of Barcelona, Barcelona, Spain.

E-mail addresses: [serena.mirra@ub.edu](mailto:serena.mirra@ub.edu) (S. Mirra), [gmarfany@ub.edu](mailto:gmarfany@ub.edu) (G. Marfany).

<https://doi.org/10.1016/j.nbd.2021.105405>

Received 17 March 2021; Received in revised form 6 May 2021; Accepted 21 May 2021

Available online 25 May 2021

0969-9961/© 2021 Published by Elsevier Inc. This is an open access article under the CC BY-NC-ND license (<http://creativecommons.org/licenses/by-nc-nd/4.0/>).

dynamics regulation have been associated with several pathological conditions, such as neurodegenerative disorders, diabetes, age-associated diseases, and lysosomal storage diseases (Yang and Klionsky, 2020; Mizushima and Levine, 2020).

The retina is endowed with an active metabolism and is particularly vulnerable to genetic and environmental alterations that cause mitochondrial dysfunction, such as impaired energy production, mtDNA instability, disturbance of mitochondrial dynamics and mitochondrial quality control (Narayan et al., 2017). These alterations make photoreceptors and retinal ganglion cells (RGCs) more susceptible to cell death and contribute significantly to the onset of retinal neurodegeneration (Eells, 2019; Mirra and Marfany, 2019).

Inherited retinal dystrophies (IRDs) are a broad group of neurodegenerative disorders associated with reduced visual capacities or even complete vision loss, which affect 1:3000 people worldwide. Retinitis Pigmentosa (RP) is the most common IRD and it is characterized by dysfunction and death of photoreceptor cells in the retina.

RP is caused by mutations in more than 70 causative genes. Among them, *CERKL* (*CERamide Kinase Like*) was first identified in a RP Spanish family (Tuson et al., 2004) and was later also associated to cone-rod dystrophy (CRD) (Aleman et al., 2009). *CERKL* is expressed in several tissues, such as brain, lung and kidney, but the retina is the tissue where *CERKL* expression is the highest. *CERKL* belongs to the ceramide kinase protein family, even though *CERKL* has never been shown to exert any kinase activity (Bornancin et al., 2005; Tuson et al., 2009). *CERKL* contains a diacylglycerol kinase domain (DAGK), a Pleckstrin homology (PH) domain, an ATP-binding domain and two nuclear localization and nuclear export signals implicated in the nucleus-cytoplasm traffic (Bornancin et al., 2005; Ali et al., 2008; Inagaki et al., 2006; Riera et al., 2013).

*CERKL* expression produces more than 20 transcripts in both human and mouse (Garanto et al., 2011). This transcriptional complexity translates to a wide range of proteins that can localize at different cellular compartments, among them cytosol, nucleus, mitochondria, Golgi vesicles and endoplasmic reticulum.

Previous functional studies performed on zebrafish embryos by knocking down *Cerkl* showed an abnormal eye development, with lamination defects in retina and increased apoptosis (Riera et al., 2013). We also generated a *Cerkl* knockdown mouse model using *cre/loxP*-mediated deletion of the first exon plus promoter. Notably, the model retained 40% of *Cerkl* expression through the use of an alternative upstream promoter. Concerning the retina, no gross morphological alterations were observed, although the RGCs function was altered in these mice (Garanto et al., 2012).

Later on we generated a complete knockout of the *Cerkl* locus using CRISPR/Cas9 (>97 kb deletion), which resulted to be lethal at embryonic stages in homozygosis (Domenech et al., 2020). Consequently, we generated a new double heterozygote model, *Cerkl*<sup>KD/KO</sup> (*KD/KO*) in which the protein expression level is below 10% of that of the wild-type retina (Domenech et al., 2020). This mouse model showed a clear phenotype of progressive retinal neurodegeneration that starts in young mice (2-month-old) and slowly progresses with age. The retinal phenotype of this *KD/KO* model is clearly detectable and includes morphological alterations such as a decreased number of cones, photoreceptor elongation, opsin mislocalization, alterations in the RPE microvilli structure and phagocytosis, and activation of gliosis markers. In young mice, there is not a detectable functional impairment of the retina. However, the electrophysiological response is strongly impaired in 18 month-old mice, thus suggesting a gradual and slow progression of visual impairment, similarly to what occurs in most patients carrying mutations in *CERKL* (Domenech et al., 2020).

*CERKL* has been described to bind several neuronal calcium sensors (Nebet et al., 2012) and sphingolipids (Garanto et al., 2013), protecting cells from oxidative stress (Tuson et al., 2009), and stabilizing the NAD-deacetylase SIRT1 to regulate general autophagy (Hu et al., 2019). Moreover, *CERKL* localizes at mitochondria where it interacts with

mitochondrial thioredoxin 2 in NIH3T3 cells (Li et al., 2014). However, the precise cellular and molecular function of *CERKL* in mammalian retina is yet to be determined.

Here we describe a pool of *CERKL* isoforms localizing at mitochondria in mouse RGCs primary culture. In addition, taking advantage of *KD/KO* in vivo model, we studied the impact of *CERKL* expression levels on mitochondrial function and mitochondrial network organization. Our results showed that retinas from *Cerkl*<sup>KD/KO</sup> model are characterized by increased autophagy that is not concomitant with increased mitophagy. Additionally, depletion of *Cerkl* causes alteration of the mitochondrial size and distribution, and dysregulation of mitochondrial metabolism and other energy-related markers.

Overall, our studies describe *CERKL* as a relevant retinal gene involved in the regulation of mitochondrial biology and metabolism, and provide a solid link between inherited retinal disorders and the alteration of cell metabolism and homeostasis in the mammalian retina.

## 2. Materials and methods

### 2.1. Animal experimentation

WT and *CERKL* transgenic lines in C57BL/6 J or Albino background were genotyped as described previously (Garanto et al., 2012; Domenech et al., 2020). Animal experiments were performed according to the ARVO statement for the use of animals in ophthalmic and vision research, as well as the regulations of the Ethical Committee for Animal Experimentation (AEC) of the Generalitat of Catalonia, according to the European Directive 2010/63/EU and other relevant guidelines.

### 2.2. Genomic DNA and genotyping by PCR

DNA for genotyping was extracted from ear punches. Primers for genotyping and PCR conditions are described in Domenech et al. (2020).

### 2.3. Retina isolation

After euthanizing the mice by cervical dislocation, eyes were enucleated and disposed in cold PBS. The neural retina was separated from the sclera, pigment epithelium and finally from the lens under a binocular Leica lens and using a pair of thin tweezers.

### 2.4. Primary cultures

Primary retinal cultures were obtained from dissection of P0-2 mouse retinas. Single cell suspension was obtained using Neural Tissue Dissociation Kit (Miltenyi Biotec, Bergisch, Gladbach, Germany). 150,000 cells were plated onto poly-D-ornithine-laminin coated coverslips in Neurobasal™-A medium (Thermo Fisher Scientific, Waltham, Massachusetts, USA) supplemented with 0.06% glucose, 0.0045% NaH<sub>2</sub>CO<sub>3</sub>, 1 mM L-glutamine, B27 1× (Invitrogen, Carlsbad, CA), penicillin/streptomycin (Invitrogen 1%), forskolin 5 μM (Sigma Aldrich, Saint Louis, Missouri, USA), BDNF 5 ng/ml (Peprotech, 450-02) and rat CNTF 20 ng/ml (Peprotech, 450-25). After 7 days of differentiation in vitro (7DIV), cells were fixed in 4% PFA for 20 min and washed 3 times with PBS 1×. If necessary, cells were stored for further experiments in cryoprotector solution (30% Glycerol, 25% Etilenglicol 100% and 0.1 M PBS). Selection of RGCs was performed as described in Domenech et al. (2020). Autophagy flux experiments were performed in vitro by adding hydroxichloroquine (HCQ, 30 μg/ml, Dolquine, Lab. Rubió, Barcelona, Spain) for 6 h to the complete culture medium to block autophagosome-lysosome fusion. To obtain hippocampal cultures E16 mouse brains were dissected in PBS containing 3% glucose and the hippocampi were dissected out. After trypsin (Invitrogen, Carlsbad, CA, USA) and DNase treatment (Roche Diagnostics), hippocampi were dissociated and cells were seeded onto 0.5 mg/ml poly-L-lysine (Sigma-Aldrich)-coated coverslips in neurobasal medium (Gibco, Grand Island, NY, USA) containing

2 mM glutamax, 120/ml penicillin, 200/ml streptomycin and B27 supplement (Invitrogen). Cells were maintained at 37 °C in the presence of 5% CO<sub>2</sub> and were cultured for between 5 and 6 days.

### 2.5. 661 W culture and plasmid constructs

CERKL-GFP was obtained by cloning the coding region of hCERKL532 cDNA (NM\_201548.4) in pEGFPN2, by using *Xho*I and BamHI restriction sites. Cone progenitor-derived 661 W cells were cultured in DMEM (Invitrogen) supplemented with 10% fetal bovine serum (FBS), 120 µg/ml penicillin and 200 µg/ml streptomycin (Life Technologies), maintained at 37 °C in the presence of 5% CO<sub>2</sub> and split at a ratio of 1:5 once per week. Upon confluence, the cells were trypsinized and 70,000 cells were seeded for each sterile glass coverslip previously coated with poly-L lysine (Sigma-Aldrich). The cells were transfected using Lipofectamin 2000 (Invitrogen) following the manufacturer's instructions and processed 48 h after transfection.

### 2.6. Immunofluorescence, confocal microscopy, and colocalization analysis

In immunocytochemistry experiments, cells were fixed in pre-chilled methanol at -20 °C for 10 min, washed in PBS (3 × 5 min), permeabilized in 0.2% Triton X-100 (St. Louis, MO, USA) in PBS (20 min at RT), and blocked for 1 h in 10% Normal Goat Serum (Roche Diagnostics) in PBS. Primary antibodies were incubated overnight at 4 °C in blocking solution. The primary antibodies used were the following: LC3 (AB BCN, Genetex; 1:1000), p62 (Abcam, ab56416, 1:500), LAMP1 (Abcam, [1D4B] ab25245, 1:500), CERKL2 and CERKL5 (Domenech et al., 2020). After incubation, coverslips with cells were rinsed in PBS 1 × (3 × 5 min), incubated with the corresponding secondary antibodies conjugated to either Alexa Fluor 488, 568 or 647 (Life Technologies, Grand Island, NY, USA) (1:400) at RT (1 h) in blocking solution. Nuclei were stained with DAPI (Roche Diagnostics, Indianapolis, IN, USA) (1:1000), washed again in PBS 1 × (3 × 5 min), mounted in Mowiol 4-88 (Merck, Darmstadt, Germany).

For immunohistochemistry experiment, eyes from adult mice were enucleated, fixed in PFA 4%, and embedded in OCT. Cryosections (12-µm section) were collected and kept frozen at -80 °C until used. Cryosections were air dried for 10 min and rehydrated with 1 × PBS (3 × 5 min) and blocked in blocking solution (1 × PBS containing 10% Normal Goat Serum and 0.3% Triton X-100 [Sigma-Aldrich]) for 1 h at room temperature. Primary antibody incubation was performed overnight at 4 °C. After three rinses with 1 × PBS (10 min each), cryosections were incubated for 1 h at room temperature with the corresponding secondary antibodies conjugated to a fluorophore. Finally, the slides were washed with 1 × PBS (3 × 10 min) and coverslipped with Fluoprep (BioMerieux, Marcy-l'Étoile, France). The primary antibodies and dilutions used included: Sestrin2 (Proteintech, I0795-I-AP; 1:500), COXIV (Invitrogen, 459,600; 1:500), LAMP1 (Abcam, [1D4B] ab25245, 1:500).

For whole-mount retina staining, retinas from adult mice were placed on glass slides photoreceptors side up, flattened by cutting the edges, fixed 1 h in 4% paraformaldehyde and rinsed with 1 × PBS (3 × 5 min). The retinas were then blocked in blocking solution (1 × PBS containing 10% Normal Goat Serum and 2% Triton X-100) for 1 h at room temperature and incubated with COXIV (Invitrogen, 459,600; 1:500) primary antibody overnight. Then they were rinsed with 1 × PBS (3 × 5 min) and incubated with Alexa Fluor 568 (Thermo Fisher Scientific, Waltham, MA) for 1 h. Retinas were washed with 1 × PBS (3 × 5 min), mounted with Fluoprep (BioMerieux).

All the samples were analyzed by confocal microscopy (Zeiss LSM 880, Thornwood, NY, USA) and images were collected using ZEN-LSM software. For quantitative analysis in both RGCs and 661 W cells, the number of the fluorescent dots (LC3 dots and p62 dots) was counted manually with ImageJ software (National Institutes of Health, Bethesda, MD). Analysis of colocalization was performed with JACoP ImageJ

plugin after images deconvolution, obtained using Huygens Deconvolution Software.

### 2.7. Transmission electron microscopy

Mice were transcardially perfused with cold fixative solution (2.5% glutaraldehyde, 2% PFA in 0.1 M phosphate buffer). Eyes were removed, retinas were dissected and fragmented in 1mm<sup>3</sup> pieces. Retinal fragments were immersed in fixative solution (2.5% glutaraldehyde, 2% PFA in 0.1 M phosphate buffer) and incubated at 4 °C overnight. Retinal fragments were post-fixed in 1% osmium tetroxide 2% K<sub>4</sub>Fe(CN)<sub>6</sub> in the dark for 2 h at 4° temperature, rinsed in double distilled water to remove the osmium. Retinal fragments were dehydrated in ascending concentrations of acetone. Then was infiltrated and embedded in Epon (EMS). Blocs were obtained after polymerisation at 60 °C for 48 h. Ultrathin sections of 60 nm in thickness were obtained using a UC6 ultramicrotome (Leica Microsystems, Austria) and were stained with 2% uranylless and lead citrate. Sections were observed in a Tecnai Spirit 120 Kv TEM, images were acquired with a 1 k × 1 k CCD Megaview camera.

### 2.8. Quantitative analyses of mitochondrial morphology

Quantitative analyses of immunofluorescence images (mitochondrial morphology in 661 W cells, RGCs cells and mitochondrial length in RGCs axons) was performed using an ImageJ software macro as described in Cherubini et al. (2015). Briefly, a binary image containing black mitochondrial structures on a white background was obtained from confocal images using the ImageJ software. From this binary image, individual mitochondria (particles) were subjected to particle analyses to acquire form factor (FF,  $(4\pi \times Am/Pm^2)$  where Pm is the length of mitochondrial outline and Am is the area of mitochondrion) and aspect ratio values (AR, the ratio between the major and minor axis of the ellipse equivalent to the mitochondrion). Mitochondrial Area in 661 W cells was calculated for each cell using the ImageJ software and normalized for the total area of the cell, labeled with cytosolic GFP green fluorescence. Quantitative analyses of TEM microphotography were performed in 26,500× images to determine mitochondrial area, mitochondrial length, mitochondrial circularity and mitochondrial aspect ratio, using the ImageJ software. Mitochondrial area represents the area occupied by each single mitochondrion; mitochondrial length represents major axis length of mitochondria; aspect ratio was obtained as major axis/minor axis. 102–123 mitochondria were analyzed from 2 WT/WT and 3 KD/KO.

### 2.9. Study of autophagy in ex vivo retinas

After adult retina dissection, half-retina sections were separately processed for study (one-half for each experimental condition, with a total of 4 experimental conditions per animal). Explants were cultured in cell culture inserts (Millipore) under control conditions [Neurobasal medium (Invitrogen) supplemented with 0.06% glucose, 0.0045% NaH<sub>2</sub>CO<sub>3</sub>, 1 Mm l-glutamine, 1 × B27 (Invitrogen, Carlsbad, CA)] and starvation conditions (Earle's Balanced Salt Solution, EBSS) in the presence or absence of HCQ (30 µg/ml, Dolquine, Lab Rubió, Barcelona, Spain). Explants were maintained for 6 h at 37 °C in the presence of 5% CO<sub>2</sub>. Successively, retinal explants were processed for western blotting analysis.

### 2.10. Western blotting

Adult retinas or retinal explants were lysed in RIPA buffer [50 mM Tris, pH 7.4, 150 mM NaCl, 1 mM EDTA, 1% NP-40, 0.25% Nadeoxycholate, protease inhibitors (Complete; Mini Protease Inhibitor Cocktail Tablets; Roche)]. Proteins were analyzed by SDS-PAGE and transferred onto nitrocellulose membranes, which were blocked with 5% non-fat dry milk in Tris-HCl-buffered saline (TBS) containing 0.1%

Tween 20, and incubated overnight at 4 °C with primary antibodies. After incubation with horseradish peroxidase-labeled secondary antibodies for 1 h at room temperature, membranes were revealed with the ECL system (Lumi-Light Western Blotting Substrate, Roche). Images were acquired by ImageQuant™ LAS 4000 mini Image Analyzer (Fujifilm) and quantified using ImageJ software. TUBULIN or GAPDH loading controls were used when needed. The primary antibodies used were the following: Beclin1 (Abcam, ab207612; 1:1000), LC3 (AB BCN, Genetex; 1:1000), VDAC (Calbiochem, (Ab-5) (185–197); 1:7000), TUBULIN (Sigma, T5168, 1:1000), GAPDH (Abcam, ab8245, 1:1000), Rodent Total OXPHOS Cocktail (MitoSciences, Eugene, OR, USA, 6 µg/ml), Sestrin2 (Proteintech, I0795-I-AP; 1:1000), MITOFUSIN2 (Abcam, ab56889, 1:1000), OPA1 (Proteintech, 27,733-1-AP, 1:1000), DRP1 (Cell Signaling Technology 14647S, 1:1000), P-DRP1 (Cell Signaling Technology, S616:3455S, 1:000). The secondary antibodies used were: HRP-labeled anti-mouse (P447-01, Vector; 1:2000) and anti-rabbit (P217-02, Vector; 1:2000).

### 2.11. Seahorse analysis

Seahorse analysis of ex vivo retinas was performed on retinal disks as described in [Kooragayala et al. \(2015\)](#). Briefly, adult neural retinas were dissected and two disks with a diameter of 1 mm were obtained from the central region of each retina, arranged onto Cell-Tak (Corning) pre-coated XF24 Islet Fluxpak mesh inserts (photoreceptors side up) and transferred to an islet plate (one disk per well) containing 450 µl of Seahorse XF Assay Medium (Seahorse Bioscience). After 1 h of incubation at 37 °C, plates were loaded into an XFe24 respirometry machine (Seahorse Bioscience). Maximum OCR was assayed with FCCP (2 µM). To inhibit complex I- and III-dependent respiration, rotenone (5 µM) and antimycin A (15 µM) were used, respectively. OCR represents the oxygen tension and ECAR acidification of the medium as a function of time (pmol min<sup>-1</sup>). 3 animals were used for each experimental condition to obtain 6 retinas and 10 retinal discs. Measurements of OCR from each disc were considered as independent value for statistical analysis.

### 2.12. DNA isolation and quantification of mtDNA content

Total DNA was isolated from retinal samples by phenol/chloroform extraction. Mitochondrial DNA (mtDNA) was quantified by real-time PCR amplification of 100 ng of total DNA using a cytochrome *b* (MT-CYTB) primer/probe set (Mm04225271\_g1). The results were expressed relative to the quantity of nuclear DNA, which was determined by amplification of the intronless gene *CEBPα* (Mm00514283\_s1) ([Villarroya et al., 2010](#)).

### 2.13. Determination of D-glucose oxidation

Retinal samples were incubated with DMEM (without D-glucose) for 1 h followed by an incubation with DMEM (without D-glucose) supplemented with 3 mM D-glucose and 1.5 µCi [<sup>14</sup>C(U)]-D-glucose (Hartmann Analytic GmbH, Braunschweig, Germany) for 3 h at 37 °C in a 5% (v/v) CO<sub>2</sub> atmosphere. Labeled <sup>14</sup>CO<sub>2</sub> was then released from the medium by acidification with 3 M HClO<sub>4</sub> and retained in a CO<sub>2</sub> trap consisting of Whatman 3MM Chr paper (Whatman, GE Healthcare, Little Chalfont, UK) impregnated with β-phenylethylamine (Sigma) and positioned over the wells inside the sealed plates. After 1 h, CO<sub>2</sub> traps were placed in scintillation vials containing 5 ml of scintillation fluid, and the samples were counted using a Packard 2100TR TriCarb Liquid Scintillation Counter (Packard Instrument Company Inc., Meriden, CT).

### 2.14. RNA isolation from retinas

Retinal samples were homogenized using a Polytron PT1200E homogenizer (Kinematica, AG, Lucerne, Switzerland). Total RNA was isolated using the RNeasy mini kit (Qiagen, Germantown, MD),

following the manufacturer's instructions.

### 2.15. Adult retinas RNA-seq

Total RNA from *Mus musculus* (Albino) retinas was quantified by Qubit® RNA BR Assay kit (Thermo Fisher Scientific) and the RNA integrity was estimated by using RNA 6000 Nano Bioanalyzer 2100 Assay (Agilent). RNASeq libraries were prepared with KAPA Stranded mRNA-Seq Illumina® Platforms Kit (Roche) following the manufacturer's recommendations. Briefly, 100–300 ng of total RNA was used for the poly-A fraction enrichment with oligo-dT magnetic beads, following the mRNA fragmentation by divalent metal cations at high temperature. The strand specificity was achieved during the second strand synthesis performed in the presence of dUTP instead of dTTP. The blunt-ended double stranded cDNA was 3'adenylated and Illumina platform compatible adaptors with unique dual indexes and unique molecular identifiers (Integrated DNA Technologies) were ligated. The ligation product was enriched with 15 PCR cycles and the final library was validated on an Agilent 2100 Bioanalyzer with the DNA 7500 assay. The libraries were sequenced on HiSeq 4000 (Illumina) with a read length of 2x76bp + 8 bp + 8 bp using HiSeq 4000 SBS kit (Illumina) and HiSeq 4000 PE Cluster kit (Illumina), following the manufacturer's protocol for dual indexing. Image analysis, base calling and quality scoring of the run were processed using the manufacturer's software Real Time Analysis (RTA 2.7.7). The read-count analysis was performed using GeneCounts option from STAR (v2.7.0d). Analysis of differentially expressed genes (DEGs) used DESeq2 v1.26.0 including principal component analysis to test for outlier samples and batch effects. One *KD/KO* sample grouped distinctly and was excluded from DEG analysis which used 2 mutant and 3 control samples. For a gene to be considered differentially expressed, we required expression change of >0.5 log<sub>2</sub> (fold change) and adjusted *p* value <0.05, plus absolute expression level of >10 counts in the sum of all conditions. Data in Supplementary Table S1 were obtained by extracting relevant genes obtained from a DESeq2 ([Love et al., 2014](#)) output of *WT/WT* vs *KD/KO* retinas and automatically annotated using DAVID (v6.8) ([Huang et al., 2009](#)).

### 2.16. cDNA synthesis and RT-PCR

cDNA was synthesized from 500 ng of total RNA using Multiscribe reverse transcriptase and random-hexamer primers (TaqMan Reverse Transcription Reagents from Applied Biosystems/Life Technologies, Foster City, CA). For mRNA expression analyses, TaqMan quantitative real-time PCR (qPCR) was performed on a 7500 Real-Time PCR System (Applied Biosystems) in a final volume of 20 ml using Platinum Quantitative PCR SuperMix-UDG with ROX reagents (Invitrogen/Life Technologies) and the *Pparg1a* (Mm01208835\_m1) and *Nr4a3* specific primer pair/probe sets. The relative levels of target mRNA expression were normalized to that of *Ppia* (Mm02342430\_g1), used as an endogenous control.

### 2.17. Caspase 3/7 activity

Caspase-9 activity was measured in retinal disks with a diameter of 1 mm (9 retinal disks from 3 animals per genotype) using a luminescence-based system (Caspase-Glo 3/7 Assay, Promega). Data were expressed as relative luminescence units (RLU).

### 2.18. Targeted metabolomic analysis

250 µg of retinas (right and left) were homogenized in 200 µl of PBS and stored at –80 °C until the moment of the analysis. After centrifugation at 1500 xg (10 min and 4 °C), the clear supernatant was used for the analysis. Amino acids were determined by tandem mass spectrometry, as previously reported ([Casado et al., 2018](#)). Briefly, amino acids were analyzed on a Waters ACQUITY UPLC H-class instrument with a

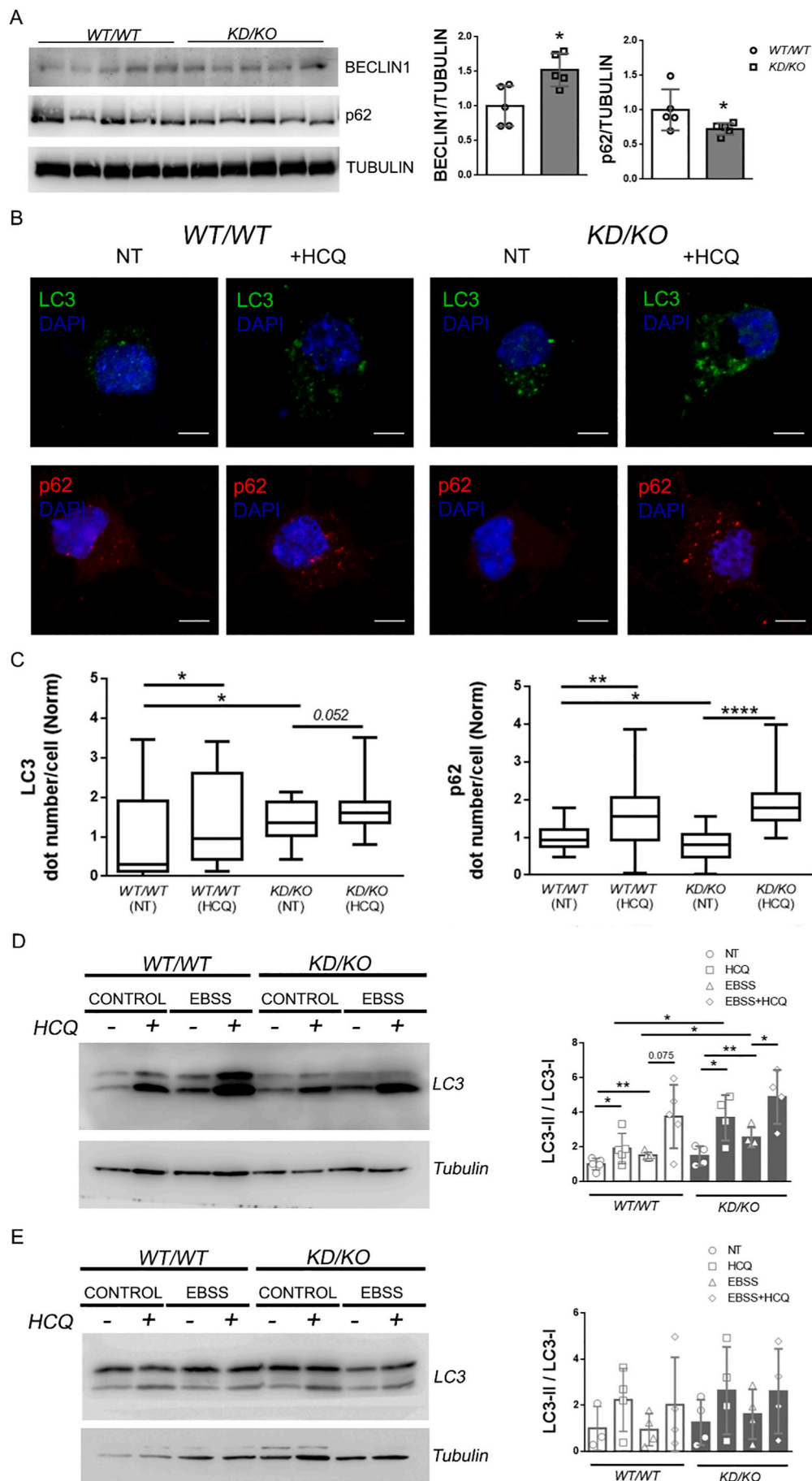


**Fig. 1. Autophagy is activated in *KD/KO* retinas.** **A)** Quantification of autophagy markers BECLIN 1 and p62 in *WT/WT* and *KD/KO* retinal lysates. ( $n = 5$  animals per genotype). **B,C)** Fluorescence microscopy detection and quantification of LC3-positive and p62-positive dots in *WT/WT* and *KD/KO* RGCs, maintained in control medium or treated with HCQ for 6 h. Scale bar 5  $\mu\text{m}$ . ( $n = 25\text{--}33$  cells for condition, from 3 to 4 animals per genotype). **D)** Western blot analysis on *WT/WT* or *KD/KO* retinal explants from 3 month-old mice and densitometric quantification of the relative intensity of LC3-II/LC3-I ratio. Retinal explants were cultured in control or starvation (EBSS) media, maintained for 6 h in the presence or absence of HCQ and then processed for LC3 detection. **E)** Western blot analysis on *WT/WT* or *KD/KO* retinal explants from 10 month-old mice (as described in D) and densitometric quantification of the relative intensity of LC3-II/LC3-I ratio. Retinal explants were cultured in control or starvation (EBSS) media, maintained for 6 h in the presence or absence of HCQ and then processed for LC3 detection. Data are shown as the mean  $\pm$  SD. Statistical analysis by Mann-Whitney test. \* $p$ -value  $\leq 0,05$ ; \*\* $p$ -value  $\leq 0,01$ ; \*\*\*\* $p$ -value  $\leq 0,001$ .

reversed-phase C-18 column using water and acetonitrile with 0.1% formic acid as the mobile phases (run time = 9 min). The detection was performed with a Waters Xevo TQD triple-quadrupole mass spectrometer using positive electrospray ionization in the multiple reaction monitoring mode. Organic acids were analyzed by Gas-Chromatography Mass spectrometry of the trimethylsilyl derivatives (BSTFA), as reported (Van Noolen et al., 2020). Briefly, after derivatisation, compounds were separated in a 60-m capillary column and detected by mass spectrometry in scan mode (to verify the nature of the compound compared with the NIST library), and quantitative mode by analyzing the response of the target ion related with that of the internal standard (undecanodioc acid). A table with the analyzed compounds is stated in Supplementary Table S2.

### 2.19. Statistical analysis

Statistical analyses were performed using the two-tailed unpaired Student's *t*-test. When data are not normally distributed, non-parametric Mann-Whitney test was used to determine the statistical significance. ROUT test was used to determine statistical outliers ( $Q = 1\%$ ). Calculations were performed with GraphPad Prism statistical software, version 6. N is shown at each Fig legend. Statistical significance was set with a value of  $p < 0.05$ , (\*  $p < 0.05$ , \*\*  $p < 0.01$ , \*\*\*  $p < 0.005$ , \*\*\*\*  $p < 0.001$ ). Data are expressed as standard deviation (SD).

## 3. Results

### 3.1. Autophagy is increased in *KD/KO* in *in vitro* and *ex-vivo* systems

To determine the potential role of CERKL in regulating autophagy in the mammalian retina we took advantage of the *Cerkl*<sup>*KD/KO*</sup> mouse model (Domenech et al., 2020). A first analysis was performed by assessing the abundance of the autophagy markers Beclin 1 and p62 by quantitative western blotting in total protein homogenates from *WT/WT* and *KD/KO* retinas (Fig. 1A). Compared to the wild-type retinas, extracts of *KD/KO* retinas showed both a significant increase in Beclin 1 and a decrease of p62 (Fig. 1A). These results indicate that autophagy is increased in *KD/KO* retinas.

To extend this result we studied autophagic flux in *WT/WT* and *KD/KO* primary cultures of retinal ganglion cells (RGCs) (P0-P2 mouse pups) maintained 7 days *in vitro* (7DIV). Cells were cultured in the absence (not treated, NT) or presence of hydroxychloroquine (+HCQ), a blocker of lysosomal degradation. After immunostaining with LC3 or p62 antibodies the numbers of isolation membranes and autophagosomes in the cytoplasm was measured (Fig. 1B–C). The number of LC3 dots in *KD/KO* was higher than in *WT/WT* cells in NT condition, whereas the number of p62 dots in *KD/KO* was lower than in *WT/WT* cells, indicating an increased autophagy in *KD/KO* RGCs, in agreement with our preliminary results (Fig. 1C). Besides, inhibition of lysosomal activity in *WT/WT* RGC cultures induced a significant increase in LC3 or p62-positive dots, indicating the existence of basal autophagy (Fig. 1C). These changes were similar in *KD/KO* retinas although with less intra-group variability than in *WT/WT* (Fig. 1C).

We next investigated autophagy in *ex vivo* retinal explants from *WT/WT* and *KD/KO* 3 month-old mice by monitoring LC3-II levels by western blot. Retinal explants were cultured in control or EBSS medium to induce starvation, and thus autophagy. Additionally, the explants were maintained 6 h in the absence (–) or presence (+) of HCQ prior processing for western blot analysis. As expected, inhibition of lysosomal activity induced an increase in LC3-II/LC3-I ratio, reflecting basal autophagy. Moreover starvation media also induced an increase in LC3-II/LC3-I ratio, an effect augmented by concomitant lysosomal inhibition (Esteban-Martínez et al., 2015). This response was globally higher in *KD/KO* retinal explants than in *WT/WT*, pointing out to an increased basal autophagy in *KD/KO* retinas (Fig. 1D), again in accordance with our previous results. Interestingly, the exacerbation of autophagic

response in *KD/KO* mice was detected in young retinas but was no longer evident in 10 month-old retinas (Fig. 1E).

In order to investigate the transcriptional changes occurring in *KD/KO* retinas, we performed RNA-seq analysis of retinal samples extracted from *WT/WT* and *KD/KO* mice. Triplicate RNA samples were prepared from the retinas of 3 different mice for genotype. After quality control and normalization of the data, we investigated how the overall expression of protein-coding genes changed in *KD/KO* retinas. However, PCA (principal component analysis) showed that one out of three *KD/KO* samples behaved as an outlier and it was excluded from subsequent analyses. We considered the differentially expressed gene when an expression change of  $>0.5 \log_2$  (fold change) is found. Hierarchical clustering was performed according to their expression values on the differentially expressed genes (DEGs) involved in autophagy to determine mice with similar DEG expression profiles; samples were clustered according to their genotype group (Fig. 2A). Among the DEG we found genes involved in both autophagy inhibition (such as *Decorin*, *Tspo*, *Pik3cg*) and activation (such as *Depp1*, *Dram1*, *Dram2*, *Sesn2*). *Sesn2* was increased in *KD/KO* (Log2Fold-Change:0,55,471) retinas. It encodes SESTRIN2, an intracellular sensor involved in a wide range of processes, such as the regulation of antioxidant defenses (by the stimulation of transcription factors such as p53, Nrf2, AP-1, and FoxOs), metabolism (by controlling AMPK and mTOR signaling), autophagy and mitophagy. It regulates autophagy by promoting the autophagic degradation of p62-dependent targets, including KEAP1, thereby up-regulating the transcription of antioxidant genes through NRF2 stabilization (Bae et al., 2013). Moreover, SESTRIN2 physically interacts with ULK1 and p62 and inhibits mTOR, thus favoring autophagy initiation (Parmigiani et al., 2014). We observed that in the retina, SESTRIN2 is mostly expressed in photoreceptors (localizing at the inner segment), the inner nuclear layer and the ganglion cell layer. SESTRIN2 expression pattern is maintained in *KD/KO* retinas (Fig. 2B), although its expression levels were increased in *KD/KO* (Fig. 2C).

### 3.2. Different pools of CERKL isoforms localize at mitochondria in retinal ganglion cells and hippocampal neurons.

CERKL has been described to localize at different cellular compartment, among them mitochondria in NIH3T3 cells, where it associates with mitochondrial thioredoxin 2 (Li et al., 2014). Moreover, it is required for autophagy in ARPE-19 cells and zebrafish models (Hu et al., 2019). CERKL can shuttle from cytosol to nucleus in response to oxidative stress conditions (Fathinajafabadi et al., 2014). However, little is known about the subcellular localization of CERKL in mammalian retina. To assess whether endogenous CERKL colocalizes with organelles involved in autophagy, we used immunofluorescence staining. 7 DIV RGCs were distinguished from other cellular populations for the presence of a large axon and the expression of TUBULIN-III- $\beta$  (Supplementary Fig. S1A). To detect CERKL we used two different in-house antibodies against peptides encoded by either exon 2 (anti-CERKL2) or exon 5 (CERKL5), which detect a different pool of endogenous isoforms (Domenech et al., 2020). CERKL isoforms did not co-localize with the lysosome marker LAMP1 or the autophagosome marker p62 (Supplementary Fig. S1B–C).

On the other hand, we observed partial colocalization with the mitochondrial marker Mitotracker (Fig. 3A). Specifically, anti-CERKL2 signal was detected in both nuclear and somatic compartments, with some colocalization with mitochondria, whereas anti-CERKL5 mainly stained isoforms localized in somatic compartment, strongly colocalizing with mitochondria. To further corroborate these results in a different neuronal system we checked the expression of CERKL in several neural tissues by using the two antibodies against CERKL. We found that each antibody recognizes distinct CERKL isoforms in tissue-dependent fashion in both developing and adult mice (Supplementary Fig. S2A–B). Thus, 3DIV hippocampal neurons from E16 mouse embryos were used to overexpress GFP-tagged CERKL (CERKL-GFP) and stain

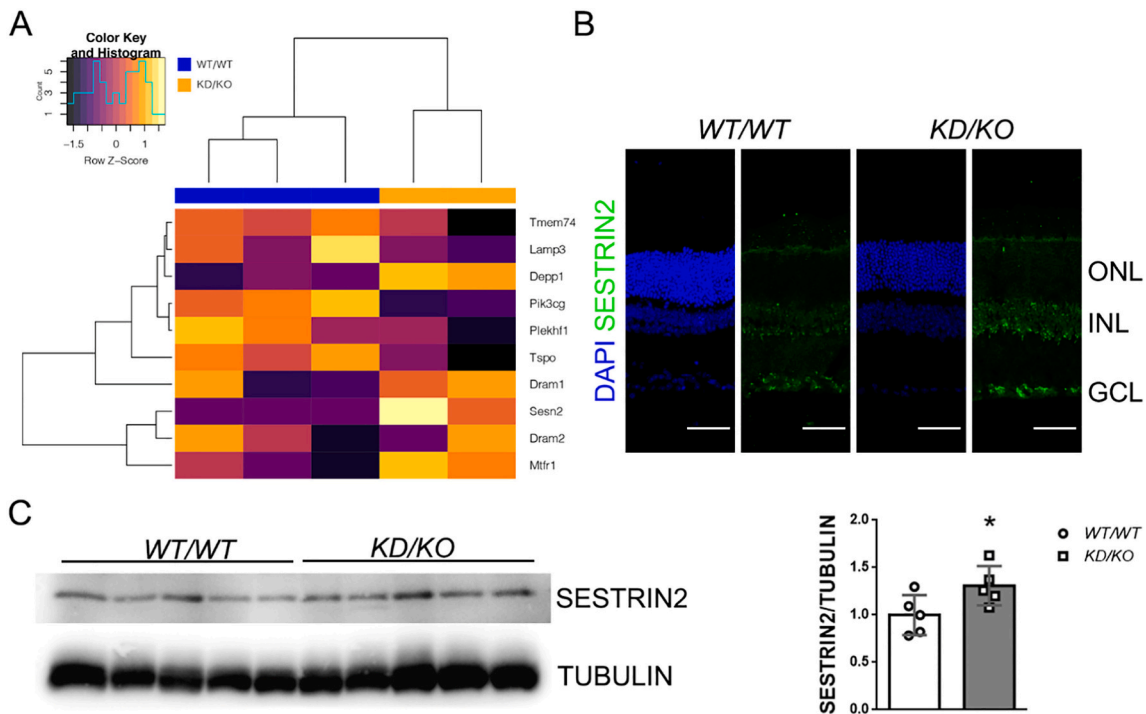


**Fig. 2.** Differential expressed genes identified by RNAseq comparing WT/WT and KD/KO retinas include genes involved in autophagy regulation. **A)** Heatmap with hierarchical clustering of differentially expressed autophagy-related genes of WT/WT (group in blue) versus KD/KO (group in orange) mouse retinas. The heatmap colours reflect the Z-score and thus differences in gene expression between samples for each of the genes selected for comparison. **B)** Immunohistochemistry of SESTRIN2 in WT/WT and KD/KO retinas. Scale bar: 50 μm. **C)** SESTRIN2 is upregulated in KD/KO retinas. ( $n = 5$  animals per genotype). Data are shown as the mean  $\pm$  SD. Statistical analysis by Mann-Whitney test. \*:  $p$ -value  $\leq 0.05$ . (For interpretation of the references to colour in this figure legend, the reader is referred to the web version of this article.)

mitochondria with Mitotracker. We observed that CERKL-GFP associated with moving mitochondria in live axons (Supplementary Fig. S2C–D). Furthermore, we confirmed the strong association of isoforms including the exon 5 epitope with mitochondria in both control and in presence of sodium arsenite to induce oxidative stress (Supplementary Fig. S3). Therefore, different pools of CERKL isoforms are associated to mitochondria undergoing mitochondrial dynamics in primary retinal ganglion cells and hippocampal neurons, with isoforms including exon 5 displaying preferential mitochondrial localization.

### 3.3. Mitochondrial mass increased in *Cerkl*<sup>KD/KO</sup> retinas

Since autophagy is the catabolic pathway able to degrade entire mitochondria, we postulated that CERKL mitochondrial localization could regulate mitochondrial total amount in retina. We first analyzed mitochondrial mass in retinas from WT/WT and KD/KO adult mice by immunostaining whole mount retinas (photoreceptors side up) for mitochondrial protein COX-IV. We found a significant increase in mitochondrial mass of KD/KO photoreceptors (Fig. 3B) and this result was further corroborated by analyzing the mitochondrial protein VDAC by western blot on total retinal homogenates (Fig. 3C). This increase in mitochondrial mass could not be attributed to an increased mitochondrial biogenesis, as the expression levels of *Pgc1a*, the major regulator of mitochondrial biogenesis, were found unaffected at level of both transcript and protein (Fig. 3D,E). Furthermore, the expression of *Nr4a3*, also essential to promote mitochondrial biogenesis was found reduced in KD/KO retinas (Fig. 3D). RNAseq analysis did not provide evidence of high differential alterations in the expression of other genes regulating mitochondrial biogenesis, although *Nrf1* and *Nfe2l2* are respectively slightly upregulated and downregulated (Supplementary Table S1).

Consequently, we checked possible changes in mitophagy. Among the different retinal layers, mitophagy has been showed to be highly

localized in vivo in the outer nuclear layer, where the soma of photoreceptors reside (McWilliams et al., 2019). Thus, we immunostained WT/WT and KD/KO retinal cryosections for COX-IV (mitochondria marker) and LAMP1 (lysosome marker) and assessed mitophagy by analyzing mitochondria-lysosomes colocalization in photoreceptors (Fig. 4A–B). Surprisingly, we did not detect any change in mitophagy by this assay (Fig. 4B).

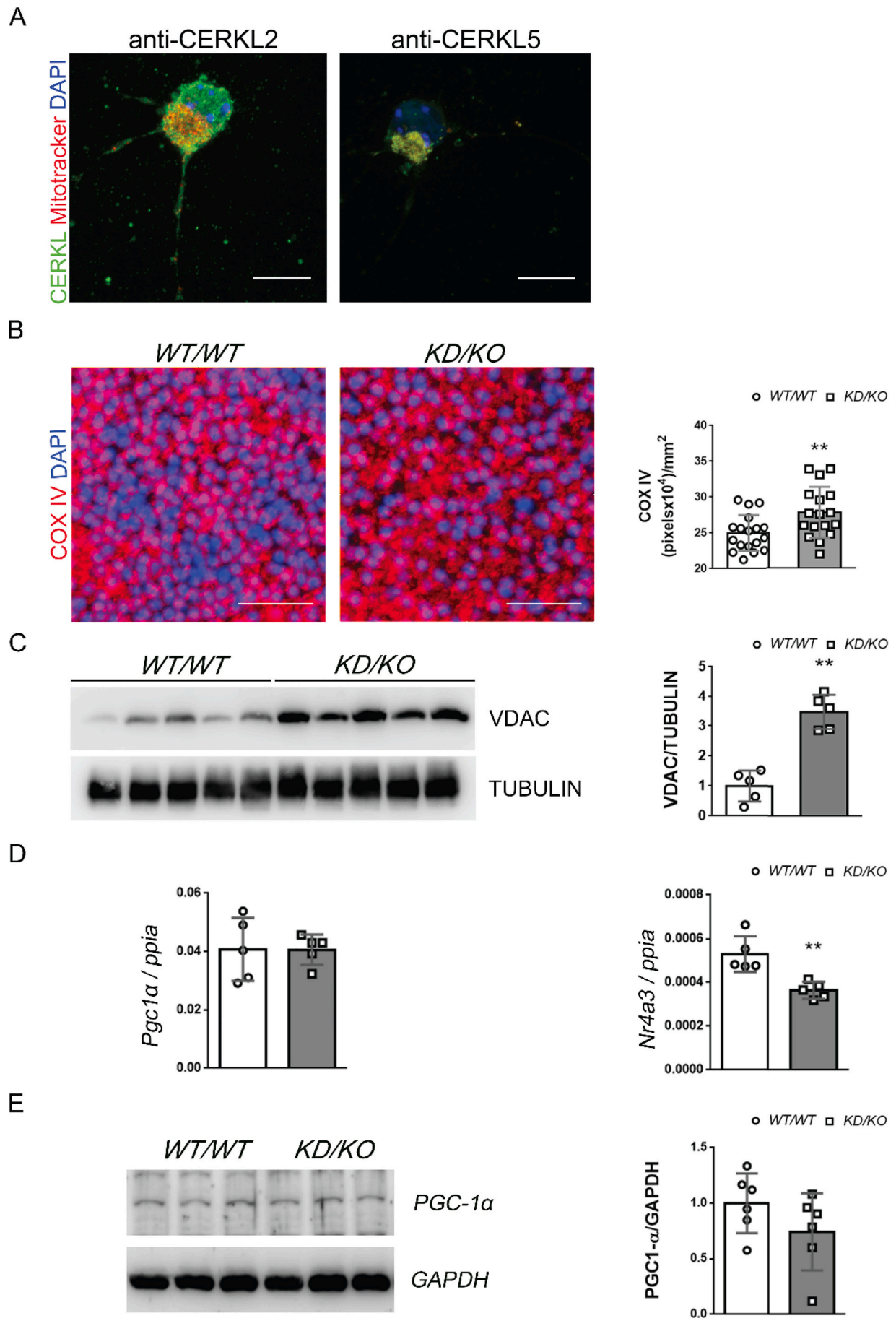
We also used WT/WT and KD/KO RGCs cultures to assess colocalization between the mitochondrial marker Mitotracker and LAMP1 in basal conditions and after blocking autophagic flux by HCQ treatment (Supplementary Fig. S4A). We observed that the colocalization coefficient in presence of HCQ was higher than in absence of HCQ, similarly in both WT/WT and KD/KO RGCs (Supplementary Fig. S4B). These results indicated that the basal level of mitophagy is not altered when *Cerkl* expression is strongly downregulated in RGCs primary cultures.

Is there any effect of the overexpression of CERKL on mitophagy? To answer this question, we transfected the 661 W photoreceptor-derived cell line with CERKL-GFP or control GFP plasmids (Fig. 4C). We observed that CERKL overexpression induced an increase in mitochondria-lysosomes colocalization (Fig. 4C), indicating that CERKL overexpression promotes mitophagy.

Overall, our data indicate that CERKL may positively regulate mitophagy, but this regulation might not be direct as it is only detected upon CERKL overexpression, whereas a strong depletion of CERKL (*Cerkl*<sup>KD/KO</sup> model) results in a global increase of general autophagy with mitophagy levels remaining similar to the WT retinas.

### 3.4. CERKL downregulation alters mitochondrial morphology and distribution

Correct mitochondrial metabolism and dynamics are essential for retinal cells and the preservation of mitochondrial function and



(caption on next page)

**Fig. 3. A pool of CERKL co-localizes with mitochondria, whose mass is increased in *KD/KO* retinas despite mitochondrial biogenesis is unaltered.** **A)** Immunofluorescence of RGCs in primary retinal cultures treated with mitochondrial marker Mitotracker and immunostained with anti-CERKL2 (green, left panels) and anti-CERKL5 (green, right panels) antibodies. Scale bar: 10  $\mu\text{m}$ . **B)** Mitochondrial immunostaining and quantification of COX-IV (red) in whole mount retinas (photoreceptors side up). Nuclei were stained with DAPI (blue). Scale bar: 20  $\mu\text{m}$ . ( $n = 18$  ROIs, 6 ROIs per animal from 3 animals per genotype). **C)** Western blot analysis and quantification of mitochondrial protein VDAC on *WT/WT* or *KD/KO* retinal homogenates. **D)** Quantitative RT-PCR for *Pgc1a* and *Nr4a3* genes in *WT/WT* or *KD/KO* retinas. **E)** Representative western blot analysis and quantification of PCG1- $\alpha$  protein on *WT/WT* and *KD/KO* retinal homogenates. In C, D and F),  $n = 5$  animals per genotype; in E),  $n = 6$  retinas from 3 animals per genotype; data are represented as the means  $\pm$  SD. Statistical analysis by Mann-Whitney test. \*:  $p$ -value  $\leq 0,05$ ; \*\*:  $p$ -value  $\leq 0,01$ . (For interpretation of the references to colour in this figure legend, the reader is referred to the web version of this article.)

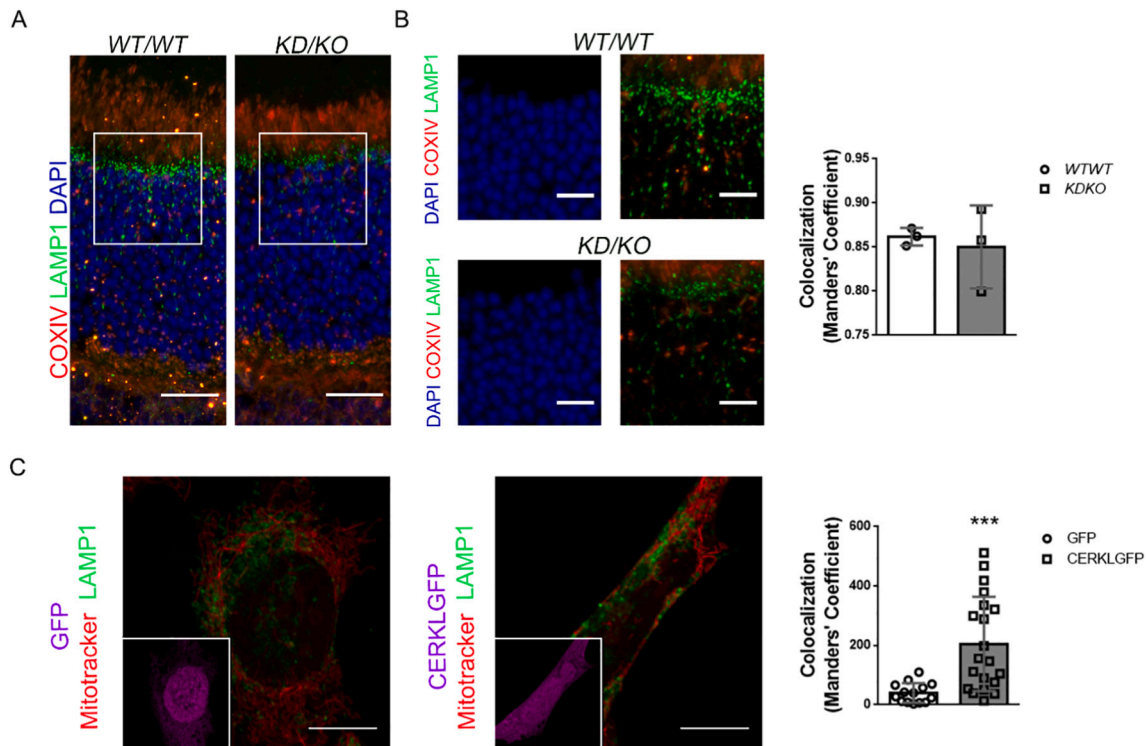


**Fig. 4. CERKL overexpression increased mitophagy in photoreceptor cell line.** **A)** Immunostaining of retinal cryosections from *WT/WT* and *KD/KO* mice with COX-IV (red) and LAMP1 (green). Scale bar: 20  $\mu\text{m}$ . **B)** ROIs such as in A) were used to assess mitophagy in photoreceptors by quantifying mitochondria-lysosomes colocalization. Scale bar: 10  $\mu\text{m}$ . ( $n = 3$  animals per genotype, 8 ROIs per animal). **C)** 661 W cells transiently expressing control GFP or CERKL-GFP (pseudo-colour in magenta, left bottom frame) were treated with Mitotracker. Scale bar: 10  $\mu\text{m}$ . Mitophagy was analyzed by measuring colocalization between Mitotracker (red) and LAMP1 (pseudo-colour in green). Scale bar: 10  $\mu\text{m}$ . ( $n = 19$ –21 cells from 2 independent experiments). Statistical analysis by Mann-Whitney test. \*\*:  $p$ -value  $\leq 0,01$ ; \*\*\*:  $p$ -value  $\leq 0,001$ . (For interpretation of the references to colour in this figure legend, the reader is referred to the web version of this article.)

morphology is required to guarantee retinal homeostasis. Since a pool of CERKL colocalizes at mitochondria and CERKL overexpression promotes mitophagy, we also aimed to assess the role of CERKL in regulating mitochondrial morphology.

To analyse the phenotypic traits of mitochondria, 7DIV RGCs from *WT/WT* and *KD/KO* P0-P1 pups were cultured and analyzed. Mitochondria were stained with Mitotracker and mitochondrial size was analyzed in proximal and distal regions of the axon (Fig. 5A). Mitochondria in *KD/KO* are shorter than in *WT/WT* in distal regions, whereas no differences in size were found in proximal regions. Notably, in *KD/KO* distal regions mitochondria are smaller than in proximal regions, indicating mitochondrial fragmentation in the regions that are farther from the soma (Fig. 5B). Moreover, we found an increased mitochondrial density in both proximal and distal regions of *KD/KO* axons (Fig. 5C). We extended our analysis to somatic mitochondria, but we were not able to detect any change in mitochondrial number and mitochondrial area (Supplementary Fig. S5A–C). Moreover, morphometric analysis revealed that mitochondria in *KD/KO* RGC somas did not display significant differences in morphological parameters such as the Aspect Ratio (AR) and Form factor (FF) in comparison to control cells (Supplementary Fig. S5D–E).

These data are indicative of alterations in mitochondrial dynamics (such as fusion, fission or trafficking) that could prevent a correct distribution of mitochondria from the soma to the more distal regions of the axon. To further study the possible alterations of mitochondrial abundance and morphology in *KD/KO* retinas we analyzed transmission electron microscopy (TEM) microphotographies from *WT/WT* and *KD/KO* RGCs and photoreceptors. In *KD/KO* RGCs we observed fragmented mitochondria characterized by irregular shapes and cristae. Moreover, autophagic structure and vacuoles were often found in *KD/KO* RGCs (Fig. 5D). From longitudinally orientated retinal samples, the IS mitochondria of *KD/KO* photoreceptors presented an abnormal morphology, with an increased circularity and a decreased maximal length and aspect ratio when compared to *WT/WT* (Fig. 5E).

To gain insight into the molecular mechanisms underlying mitochondrial fragmentation in *KD/KO* retinas, we analyzed the expression of the mitochondrial fusion/fission main regulators MITOFUSIN2, OPA1 and DRP1. The mitochondrial fusion protein MITOFUSIN2 is down-regulated in *KD/KO* retinas (Fig. 5F), suggesting that mitochondrial fusion might be altered upon *Cerkl* depletion.

Overall, our data indicated that *Cerkl* expression levels regulate mitochondrial number, morphology and distribution in different

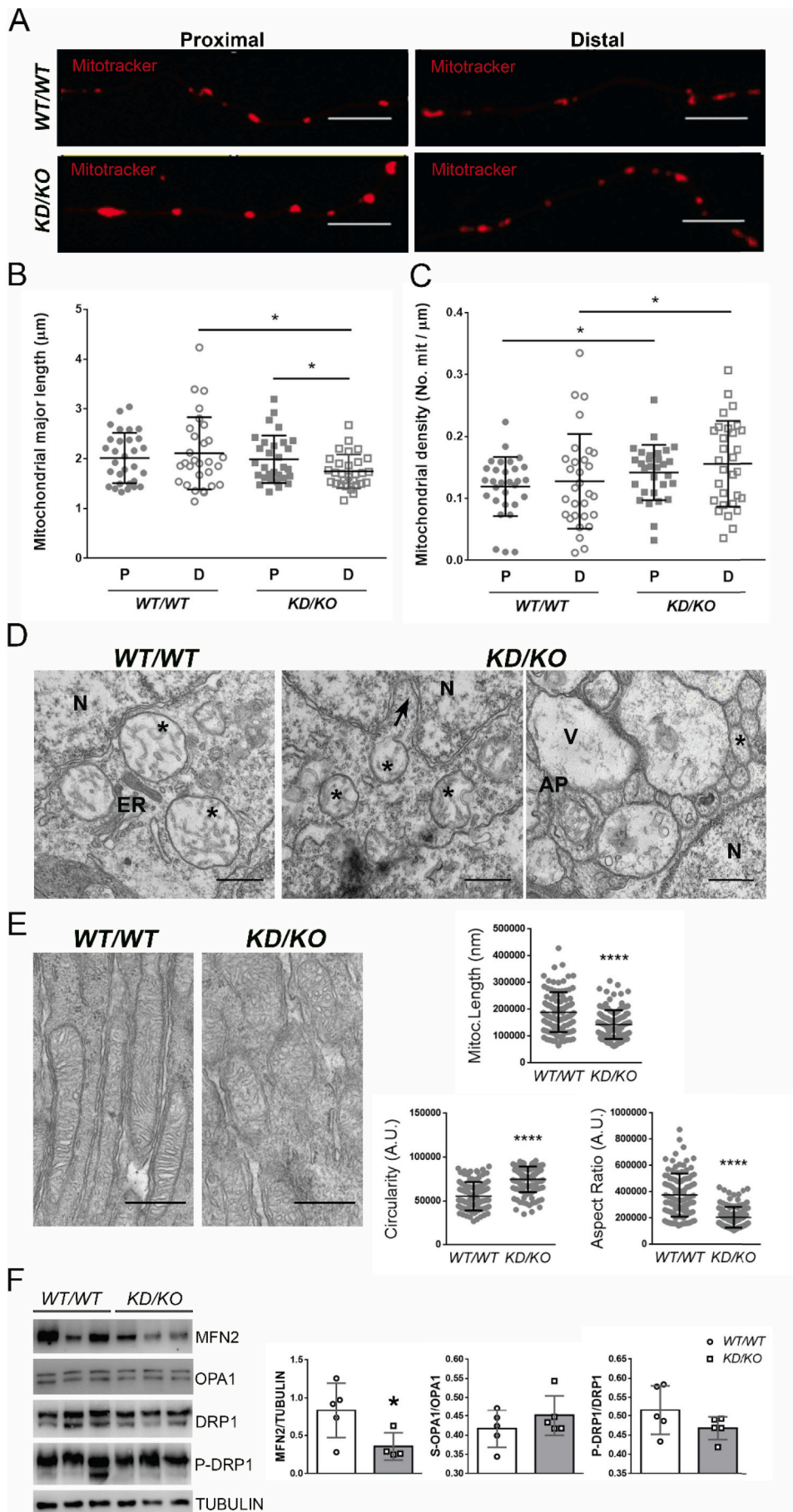


**Fig. 5. Differential mitochondrial morphology and distribution of in *Cerkl* KD/KO retinas compared to WT/WT.** A) Representative confocal images of proximal (20  $\mu\text{m}$  from the soma) and distal (100  $\mu\text{m}$  from the soma) axon regions of WT/WT and KD/KO RGCs. Mitotracker was used to detect mitochondria (red). Scale bar: 10  $\mu\text{m}$ . B) Quantification of mitochondrial major length in proximal and distal axon regions of WT/WT and KD/KO RGCs. C) Quantification of mitochondrial density in proximal and distal axon regions of WT/WT and KD/KO RGCs. ( $n = 30$  cells from 4 to 6 animals per genotype). Statistical analysis by Mann-Whitney test. \*:  $p$ -value  $\leq 0,05$ ; \*\*:  $p$ -value  $\leq 0,01$  D) TEM microphotographies from WT/WT and KD/KO retinas. Control cells displaying normal mitochondria (\*) and endoplasmic reticulum (ER). Mitochondria (\*) in KD/KO RGCs are smaller, with irregular membrane shape cristae; invaginations in nuclear membrane (arrow), large vacuoles (V) and autophagy events (AP) are detected in KD/KO RGCs. Scale bar: 1  $\mu\text{m}$ . E) TEM microphotographies were used to quantify mitochondrial length, circularity and aspect ratio in the inner segment. Scale bar: 1  $\mu\text{m}$ . Data are represented as the means  $\pm$  SD. ( $n = 12$  images with a total of 102–123 mitochondria, from 2 WT/WT and 3 KD/KO). Statistical analysis by Mann-Whitney test or 2-tailed Ttest \*\*\*\*:  $p$ -value  $\leq 0,0001$ . F) Representative western blot analysis and quantification of MITOFUSIN2, OPA1, P-DRP1 and total DRP1 proteins on WT/WT and KD/KO retinal homogenates.  $n = 4$ –5 animals per genotype; data are represented as the means  $\pm$  SD. Statistical analysis by Mann-Whitney test. \*:  $p$ -value  $\leq 0,05$ . (For interpretation of the references to colour in this figure legend, the reader is referred to the web version of this article.)

cellular population of mammalian retina.

### 3.5. Oxygen consumption and energy related is impaired in *KD/KO* retinas

The retina is a highly metabolic tissue, generating adenosine triphosphate (ATP) via glycolysis in the cytosol or via oxidative phosphorylation in mitochondria. Seahorse analysis on *KD/KO* and *WT/WT* retinal explants allowed us to measure changes in oxygen consumption rates (OCR), as an index of mitochondrial respiration, as well as extracellular acidification rates (ECAR), as an index of glycolysis. Our results clearly support that *KD/KO* retinal explants show a strong decrease in OCR when compared with *WT/WT* retinas (Fig. 6A). Indeed, basal respiration, maximal respiration and spare capacity are all compromised in *KD/KO* explants (Fig. 6B). On the other hand, the ECAR remained equivalent between *KD/KO* and *WT/WT* (Fig. 6C). Moreover, we checked if glucose oxidation might be altered in *KD/KO* retinas but no significant differences were found with respect to *WT/WT* retinas (Fig. 6D).

We next wondered whether this decrease in oxygen consumption rates was associated with a decrease in mitochondrial DNA copy number in *Cerkl*-depleted retinas. Retinal extracts from *WT/WT* and *KD/KO* retinas were used to determine mtDNA-encoded *CYTB* copy number, which tended to be higher in *KD/KO* retinas compared with wild type situation, but without reaching statistical significance (Fig. 6E).

In order to explore whether alterations in mitochondrial morphology and respiration may result in apoptotic activation, we measured caspase 3/7 activity in retinal disks from *WT/WT* and *KD/KO* retinas. Our results clearly indicated a significant increase in apoptosis in *KD/KO*, which could be associated to this decrease in mitochondrial function (Fig. 6F). We next analyzed possible changes in the abundance of total mitochondrial content and to this end, several OXPHOS proteins were immunodetected and quantified in retinal extracts from *WT/WT* and *KD/KO* retinas (Fig. 6G). As previously observed, VDAC protein levels supported an overall increase in mitochondrial content. Additionally, we observed significant increase in CIII-UQCRC2, while CII-SDHB levels tend to decrease. No changes were found in the expression of other OXPHOS proteins (CV-ATP5A, CII-SDHB, CI-NDUFB8) (Fig. 6H), suggesting differential modulation of structural and functional mitochondrial proteins.

### 3.6. *KD/KO* retinas display altered metabolism

In order to understand the metabolic changes in *KD/KO* retinas we further analyzed the RNAseq data. We found several downregulated genes involved in lipid metabolism (such as *Abca9* and *Hacd4*) as well energy metabolism related-genes (such as *Suclg*, *Ndufa4l2*, *Cox8b* or several *Slc* genes) (Fig. 7 A–B). Other mitochondrial-related genes showed a significant adjusted *p* value ( $< 0.05$ ), even though the change of their expression was considered below the stringent threshold levels used for cut-off ( $< 0.5 \log_2\text{Fc}$ ), (Fig. 7C and Supplementary Table S1).

Thus, we applied targeted metabolomic analysis to reveal if such changes may have an impact in energy metabolism related biomarkers analyzed in the retina.

After the quantitative analysis of amino acids, no significant changes were observed when we compared *WT/WT* and *KD/KO* model. Regarding organic acids, after the analysis of a large list of metabolites related with energy metabolism (Supplementary Table S2), succinate was found increased in the *KD/KO* retinas, but no other Krebs cycle metabolites or lactate (Fig. 7C). A second molecule that was significantly different when we compared both populations was piroglutamic acid, which was significantly higher in the *KD/KO* (Fig. 7C).

## 4. Discussion

In this work we took advantage of the double heterozygote *Cerkl*<sup>*KD*</sup>/

*KO* model to describe for the first time the cellular scenario originated by the impairment of CERKL function in the mammalian retina. The retina, one of the most metabolically active regions of the central nervous system, is continuously subject to light stress and oxidative injury, which are extremely damaging to neurons and compromise retinal function. Photoreceptor and retinal ganglion cells are the retinal cell types most susceptible to apoptosis and their survival depends on the action of cell resilience and anti-apoptotic mechanisms to prevent premature death. We here provide strong evidence of mitochondrial localization of CERKL in the mammalian retina. In particular, CERKL isoforms containing exon 5 strongly localize at mitochondria. Interestingly, the *Cerkl* protein sequence does not include any mitochondrial localization signal. However, exon 5 encodes a domain with an ATP-binding site that is conserved in vertebrates (Riera et al., 2013). Of note, the most prevalent RP mutation (R283X) is in exon 5, highlighting the importance of mitochondrial localization of CERKL. Given the very dynamic nature of CERKL subcellular localization, we postulated that a certain pool of CERKL isoforms (especially those including exon 5) can be recruited at mitochondria at basal level and/or in response to certain stimuli. CERKL had been already reported to interact with TRX2 at mitochondria in NIH3T3 cells, regulating the mitochondrial peroxiredoxin-mediated antioxidant pathway (Li et al., 2014). In view of our results, CERKL may be also recruited to mitochondria by interacting with additional scaffold mitochondrial proteins.

We wondered if *Cerkl* downregulation could have an impact on mitochondrial function. Mitochondria supply energy to the cell through oxidative phosphorylation (OXPHOS), which result to be more advantageous in terms of energetic yield if compared with glycolysis. It has been shown that photoreceptor mitochondria perform at their maximal respiratory capacity, with limited reserve below 25% (Kooragayala et al., 2015). Consequently, photoreceptors are very sensitive to alterations in aerobic energy metabolism and their survival closely depends on metabolic homeostasis. Our data points to the ability of CERKL to functionally impact mitochondrial respiration but not glycolysis or glucose oxidation in retina. In *Cerkl*-depleted retinas, the bioenergetics decrease detected by Seahorse is supported by changes in the levels of proteins from different complexes of the OXPHOS system. Moreover, we observed transcriptional changes in several OXPHOS genes (Fig. 7B–C).

Targeted metabolomic analysis revealed that most energy-related metabolites were not different when we compared *WT/WT* and *KD/KO* retinas. It was not a surprise since this observation has been consistently reported in humans with different mitochondrial disorders of genetic origin. Interestingly, succinate was significantly higher in *KD/KO*. Two hypotheses may explain these results: i) the decreased expression of *Suclg2* gene detected in RNAseq analysis; *Suclg2* encodes the succinate-Coenzyme A ligase, which metabolize succinate to succinyl-CoA in a reversible reaction coupled to GDP/GTP; ii) the slight reduction observed in mitochondrial complex II protein. In any case, succinate is a metabolite with pleiotropic properties, since it has been involved in energy metabolism, in regulation of ketone body utilization, ROS homeostasis, tumorigenesis, inflammation or hypoxia, among other conditions (Tretter et al., 2016). Piroglutamic acid, a precursor of glutathione, was also increased in *KD/KO*. Although no evidences were observed after RNAseq analysis in the genes related with the glutathione cycle, this finding might reflect an increased glutathione biosynthesis to cope with the increased ROS generation in *Cerkl*-mutant retinas.

Our findings point out a state of metabolic stress in *KD/KO* retinas, which could have strong negative effects on photoreceptors homeostasis. Indeed, studies performed in 661 W cells showed that changes in energy metabolism correlates with the amount of subsequent cell death (Perron et al., 2013). Previous work showed that CERKL overexpression protects cells from apoptosis and that its downregulation induce apoptosis-like cell death in zebrafish (Tuson et al., 2009; Riera et al., 2013). Interestingly, we were able to detect retinal cell death through analysis of caspase 3/7 activity, which significantly increased in *KD/KO* retinal explants. The initiation of apoptosis at this stage could be

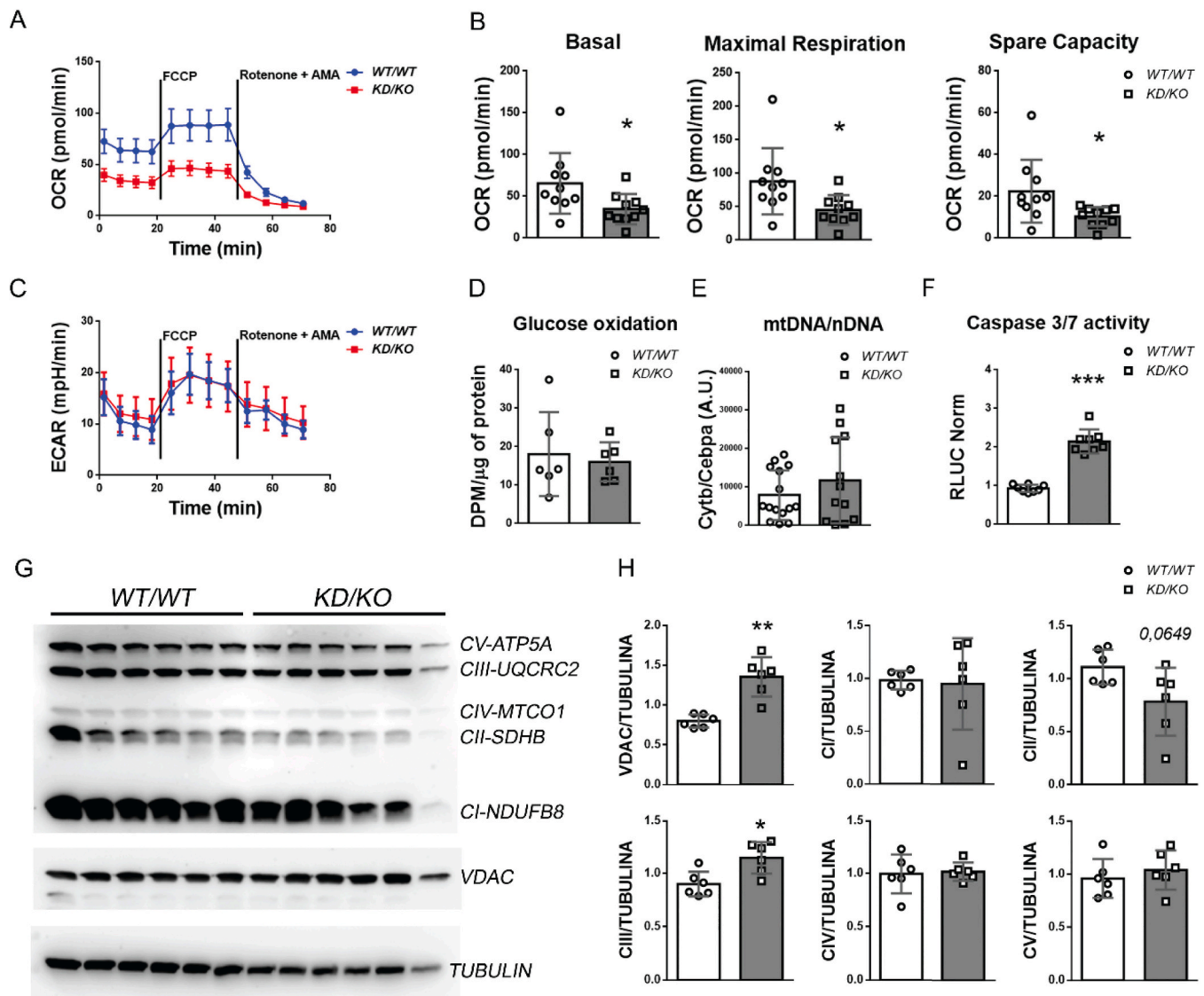


**Fig. 6. Oxygen consumption impairment in *KD/KO* retinas.** A) Diminished oxygen consumption rate (OCR) in *KD/KO* retinas compared to *WT/WT* as measured by Seahorse XF24 Analyzer. B) Basal: initial OCR without treatment; maximal respiration: after addition of FCCP (carbonyl cyanide-4-trifluoromethoxy phenylhydrazine); spare capacity: calculated by subtracting basal respiration from maximal respiratory capacity. Treatment with rotenone and antimycin A (AMA) reveals non-mitochondrial respiration. C) No differences in extracellular acidification response (ECAR) were detected between genotypes in the same experiment of A). A) to C) ( $n = 10$  retinal disks from 3 animals per genotype). D) Glucose uptake in *WT/WT* and *KD/KO* retinas were detected by a glucose oxidation assay. ( $n = 6$  retinas from 3 animals per genotype). E) mtDNA relative abundance in *WT/WT* and *KD/KO* retinas. ( $n = 12-15$  retinas from 6 to 8 animals per genotype). Statistical analysis in A) to E) was performed with 2-tailed Student's *t*-test and represented as the means  $\pm$  SEM. F) Caspase 3/7 activity in *WT/WT* and *KD/KO* retinal disks. ( $n = 9$  retinal disks from 3 animals per genotype). Statistical analysis by Mann-Whitney test. \*\*\*:  $p$ -value  $\leq 0,001$  G) Western blots of OXPHOS proteins and VDAC in *WT/WT* and *KD/KO* retinas. H) Densitometric quantification of mitochondrial proteins. ( $n = 6$  retinas from 3 animals per genotype). Data are represented as the means  $\pm$  SD. Statistical analysis was performed with Mann-Whitney test. \*:  $p$ -value  $\leq 0,05$ ; \*\*:  $p$ -value  $\leq 0,01$ .

considered the beginning of the neurodegenerative process that could progress with age, thus inducing neuroinflammation, photoreceptor loss and finally culminating in the visual impairment characterizing *Cerkl<sup>KD/KO</sup>* aged mice (Domenech et al., 2020).

Energy depletion usually generates oxidative stress conditions, mitochondrial depolarization and mitochondrial damage. Interestingly, mitochondrial dysfunction has been found in retinas of relatively young *KD/KO* mice (3-month old) and could represent a metabolic trigger for the wide set of cellular alteration observed in this study. Indeed, in a global scenario of metabolic dysfunction, the activation of autophagy can be interpreted as a stereotyped response to restore cellular homeostasis by: i) supplying the cell with the nutrients and energy in order to

compensate metabolic imbalance; ii) eliminating cellular components and organelles that are damaged by oxidative stress arising from mitochondrial dysfunction; iii) activating anti-oxidant response by inducing of p62/Keap1/Nrf2 system. Interestingly, RNAseq analysis provided several differentially regulated genes that are involved in the anti-oxidant response through autophagy regulation. Among them, *Depp* is an hypoxia-induced gene involved in autophagy that mediates autophagosome formation (Salcher et al., 2017; Stepp et al., 2014); *Tspo* is an outer-mitochondrial membrane protein that acts as redox regulator of cell mitophagy and lipophagy (Kim et al., 2020; Scaini et al., 2019; Gatiloff and Campanella, 2015); *Dram1* is a lysosomal membrane protein that is required for the autophagy induction via inhibition of P3K-AKT-

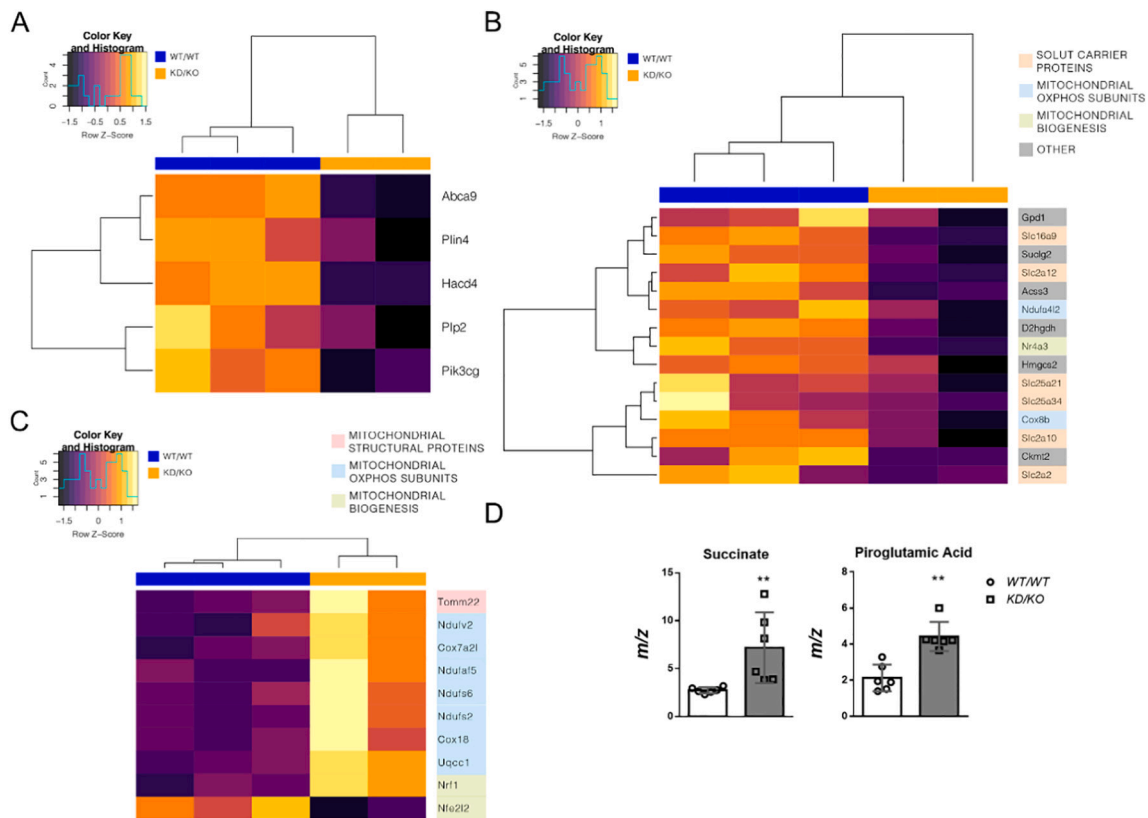


**Fig. 7.** A–B) Heatmap with hierarchical clustering of differentially expressed lipid-related (A) and mitochondrial-energy-related genes (B) of WT/WT (group in blue) versus KD/KO (group in orange) mouse retinas. C) Graphical representation of mitochondrial biology-related genes with a significant adjusted  $p$  value ( $< 0.05$ ) which were not included in B) because of their lower  $\log_2 F_c$  values ( $< 0.5$ ). The heatmap colours reflect differences in gene expression between the group of genes selected for comparison but are not directly related to the global gene expression levels. D) Targeted metabolomic analysis revealed changes in succinate and piroglutamic acid in the KD/KO retinas. Data are shown as the mean  $\pm$  SD. Statistical analysis by Mann-Whitney test. \*\*:  $p$ -value  $\leq 0.01$ . (For interpretation of the references to colour in this figure legend, the reader is referred to the web version of this article.)

mTOR-S6 pathway among others (Lu et al., 2019; Wu et al., 2018; Nagata et al., 2018); *Dram2* induces autophagy in a p53-dependent manner, and its mutations are causative of autosomal recessive adult-onset cone-rod dystrophy (Abad-Morales et al., 2019; Yoon et al., 2012); and *Sestrin2* is induced upon stressful conditions to sustain NRF2 activation and activates autophagy by both inhibiting mTORC1 and activating AMPK (Bae et al., 2013; Parmigiani et al., 2014; Morsch et al., 2019). Interestingly, SESTRIN2 was expressed in the inner segment of photoreceptors, where mitochondria are mainly localized.

The scarcity of data concerning the molecular function of CERKL includes the notion that CERKL interacts with SIRT1, one of the main regulators of acetylation/deacetylation in autophagy (Hu et al., 2019). In Zebrafish *Cerkl*-depleted retinas SIRT1 was downregulated as they were its targets ATG5 and ATG7 (both showing a higher degree of acetylation); as a consequence, autophagy decreased (Hu et al., 2019). We also observed a decrease in SIRT1 protein levels in in KD/KO mouse retinas (Supplementary Fig. S6), suggesting that additional molecular mechanisms contribute to autophagy regulation in mammalian retina. Therefore, further studies are required to outline the role of CERKL-SIRT1 interaction in mammalian retina and the mechanisms of autophagy induction.

In recent years multiple findings have shed light on the important role of autophagy in the maintenance of photoreceptor homeostasis and therefore, of visual function (Boya et al., 2016). Autophagy alterations have been related with RP, but the evidence regarding its role in the disease is controversial, probably due to both the wide heterogeneity of this pathology and the different roles that autophagy may play in the death of rods and cones. Moreover, autophagy is usually beneficial under low levels of stress but may be deleterious when the stress

dramatically increases, thus leading to cell death and degeneration (Chen et al., 2013; Punzo et al., 2009; Zaninello et al., 2020). Our data demonstrate an increased basal autophagy that is also concomitant with cell death, probably at the early stages of neurodegeneration, given the absence of visual impairment at the phenotypic level in young animals (Domenech et al., 2020). It may represent either a residual attempt to restore cellular homeostasis and/or a first manifestation of cell death commitment.

The phenotype of mitochondrial fragmentation in KD/KO is indicative of alterations in mitochondrial dynamics, such as an increased fission, a decreased fusion and/or alteration in mitochondrial trafficking along the axons. Alterations in mitochondrial dynamics may cause cytoarchitectural changes previously observed in KD/KO RGCs, which included axon shortening and dendritic arbor expansion (Domenech et al., 2020). However, we have not observed transcriptional changes in the more conventional and well characterized molecular pathways regulating mitochondrial morphology (Supplementary Table S1). However, the alteration in mitochondrial morphology may derive from changes in the protein levels or post-translational modification. Consistently, we found that MITOFUSIN2 is downregulated in KD/KO retinas. Further work will determine the mechanism of CERKL role in the regulation of mitochondrial morphology.

Global alteration in mitochondrial dynamics could be a consequence of mitochondrial dysfunction. Indeed, a wide set of findings support the model that mitochondrial fission promote the segregation of damaged mitochondria and facilitate their clearance by mitophagy (Twig et al., 2008; Ashrafi and Schwarz, 2012; Buhlman et al., 2014). By using different in vitro and ex vivo approaches, we demonstrated that general autophagy is increased in KD/KO retinas. Accumulation of mitochondria

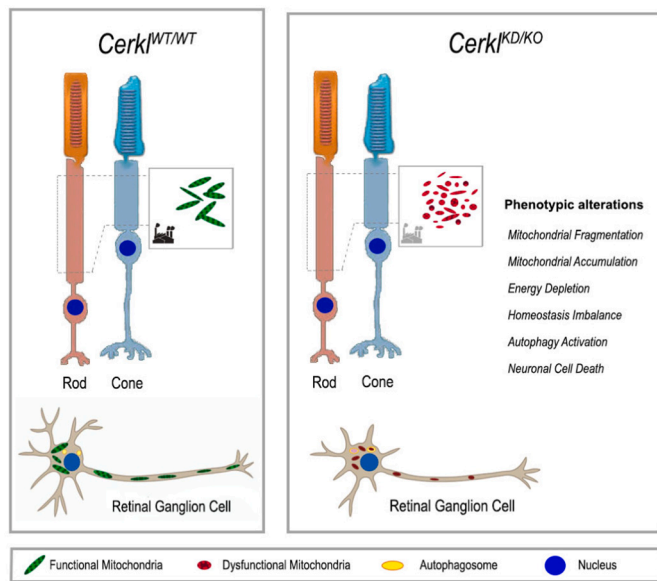


**Fig. 8.** Model for the altered cellular phenotype observed in *Cerkl*<sup>KD/KO</sup> photoreceptors and retinal ganglion cells. Depletion of *Cerkl* expression increased mitochondrial content in *Cerkl*<sup>KD/KO</sup> photoreceptors, concomitant to mitochondrial dysfunction in *Cerkl*<sup>KD/KO</sup> retina and increased autophagy activation, thus reflecting homeostasis imbalance. Cell death was also increased in *Cerkl*<sup>KD/KO</sup> retinal explants.

is not accompanied by a massive induction of mitochondrial biogenesis pathways; thus, we hypothesize a loss of the synergic modulation between mitochondrial biogenesis and mitochondrial clearance in *KD/KO* retinas. Nevertheless, this strong response in activating autophagy does not correlate with an increased mitophagy neither in vivo in photoreceptors nor in vitro in RGCs. In spite the recent generation of reliable tools to analyzing mitophagy in vivo, the assessment of mitochondrial selective autophagy in the retina remains challenging (McWilliams et al., 2019; Rosignol et al., 2020). However, data coming from CERKL overexpression in 661 W photoreceptor-derived cell line support that CERKL increases mitophagy and allows to postulate that its depletion could prevent mitophagy. This possibility is supported by the increase in mitochondrial content observed in *KD/KO* retinas. Those mechanisms would be necessary to ensure a neuroprotective effect in a context of strong metabolic dysfunction. Our proposed model for the cellular phenotype observed in *Cerkl*<sup>KD/KO</sup> photoreceptors and ganglion cells is summarized in Fig. 8. Depletion of *Cerkl* expression induced mitochondrial dysfunction that cannot be compensated by synergic modulation of mitophagy and mitochondrial biogenesis. In this context cellular metabolism and homeostasis are impaired, autophagy increases, and cells start to undergo apoptosis.

Additionally, *Cerkl*<sup>KD/KO</sup> RGCs showed alterations in axonal mitochondrial morphology and distribution, which probably resulted in the cytoarchitectural changes observed (previous work, (Domenech et al., 2020)), such as increased number of neurites and shortened axons.

An increasing number of studies report novel mechanisms and molecular actors regulating mitochondrial dynamics and function, which are essential in central nervous system in both physiological processes and disease conditions (Khacho and Slack, 2018; Mirra et al., 2016; Yang et al., 2020; Zhang et al., 2020). Consequently, mitochondria represent a promising therapeutic target, and several therapeutical strategies have been reported to act on mitochondrial related retinal diseases. These strategies include gene therapy, microRNA, genome editing, optogenetics, and stem cell-mediated mitochondrial donation (Carrella et al., 2020; Jiang et al., 2019). Moreover, the functional characterizations of metabolic and signaling pathways that are altered by mutations in RP causative genes are essential to face the great challenge of designing

efficient therapeutic strategies. Our results here provide a list of mitochondrial metabolic pathways altered by *CERKL* mutations that are worth exploring. We propose that restoring homeostasis and mitochondrial function in some IRDs may increase photoreceptor resilience and thus slow down, or even halt, the progress of retinal neurodegeneration.

## 5. Conclusions

In conclusion, our results support that the retinal degeneration *CERKL* gene is a regulator of mitochondrial biology with a retinal resilience role. *Cerkl* downregulation has an impact on mitochondrial morphology, dynamics, and mitochondria-energy-related processes. We propose a model to explain why mutations in this gene leads to severe retinal cell death in Retinitis Pigmentosa and CRD. This study opens novel therapeutic avenues based on a metabolic intervention approach to treat retinal neurodegeneration.

Supplementary data to this article can be found online at <https://doi.org/10.1016/j.nbd.2021.105405>.

## Competing interests

No competing interests declared.

## Credit author statement

S.M. and R.G-A performed the cell biology experiments; E.B-D, C-H-U and J.G-F. performed RNA-Seq and transcriptomics analysis; A.G-N and F.V. performed the bioenergetics assays; R.A and C-O performed the metabolomics analyses; S.M. and G.M designed and supervised the experimental work. S.M., J.F.G, R.A, F.V. and G.M provided the funding. S.M. wrote the manuscript draft and all authors revised and discussed the text.

## Acknowledgements

We are grateful to the associations of patients affected by retinal dystrophies for their constant support. We also acknowledge past and present members of our research group for helpful discussions. S.M. has a postdoctoral contract with CIBERER/ISCIII, R.G-A. received a research initiation contract (IBUB, 2020) and has a FI grant (Generalitat de Catalunya); E.B-D was recipient of a FI grant (Generalitat de Catalunya). This research was supported by grants ACCI 2019 (CIBERER /ISCIII) to S.M. and R.A.; SAF2016-80937-R (Ministerio de Economía y Competitividad/ FEDER) and PID2019-108578RB-I00 (Ministerio de Ciencia e Innovación/ FEDER) to G.M.; SAF2017-85722-R from (Ministerio de Ciencia e Innovación) to F.V.

## References

- Abad-Morales, V., Burés-Jelstrup, A., Navarro, R., Ruiz-Nogales, S., Méndez-Vendrell, P., Corcóstequi, B., Pomares, E., 2019. Characterization of the cone-rod dystrophy retinal phenotype caused by novel homozygous DRAM2 mutations. *Exp. Eye Res.* 187, 107752. <https://doi.org/10.1016/j.exer.2019.107752>.
- Aleman, T.S., Soumitra, N., Cideciyan, A.V., Sumaroka, A.M., Ramprasad, V.L., Herrera, W., Windsor, E.A.M., Schwartz, S.B., Russell, R.C., Roman, A.J., Inglehearn, C.F., Kumaramanickavel, G., Stone, E.M., Fishman, G.A., Jacobson, S.G., 2009. CERKL mutations cause an autosomal recessive cone-rod dystrophy with inner retinopathy. *Investig. Ophthalmol. Vis. Sci.* 50, 5944–5954. <https://doi.org/10.1167/iovs.09-3982>.
- Ali, M., Ramprasad, V.L., Soumitra, N., Mohamed, M.D., Jafri, H., Rashid, Y., Danciger, M., McKibbin, M., Kumaramanickavel, G., Inglehearn, C.F., 2008. A missense mutation in the nuclear localization signal sequence of CERKL (p.R106S) causes autosomal recessive retinal degeneration. *Mol. Vis.* 14, 1960–1964. <http://www.ncbi.nlm.nih.gov/pubmed/18978954> (accessed May 1, 2020).
- Ashrafi, G., Schwarz, T.L., 2012. The pathways of mitophagy for quality control and clearance of mitochondria. *Cell Death Differ.* 20, 31–42. <https://doi.org/10.1038/cdd.2012.81>.
- Bae, S.H., Sung, S.H., Oh, S.Y., Lim, J.M., Lee, S.K., Park, Y.N., Lee, H.E., Kang, D., Rhee, S.G., 2013. Sestrins activate Nrf2 by promoting p62-dependent autophagic

- degradation of keap1 and prevent oxidative liver damage. *Cell Metab.* 17, 73–84. <https://doi.org/10.1016/j.cmet.2012.12.002>.
- Bornancin, F., Mechtcheriakova, D., Stora, S., Graf, C., Wlachs, A., Dévay, P., Urtz, N., Baumrucker, T., Billich, A., 2005. Characterization of a ceramide kinase-like protein. *Biochim. Biophys. Acta Mol. Cell Biol. Lipids* 1687, 31–43. <https://doi.org/10.1016/j.bbalip.2004.11.012>.
- Boya, P., Reggiori, F., Codogno, P., 2013. Emerging regulation and functions of autophagy. *Nat. Cell Biol.* 15, 713–720. <https://doi.org/10.1038/ncb2788>.
- Boya, P., Esteban-Martínez, L., Serrano-Puebla, A., Gómez-Sintes, R., Villarejo-Zori, B., 2016. Autophagy in the eye: development, degeneration, and aging. *Prog. Retin. Eye Res.* 55, 206–245. <https://doi.org/10.1016/j.preteyeres.2016.08.001>.
- Buhlman, L., Damiano, M., Bertolin, G., Ferrando-Miguel, R., Lombès, A., Brice, A., Corti, O., 2014. Functional interplay between Parkin and Drp1 in mitochondrial fission and clearance. *Biochim. Biophys. Acta, Mol. Cell Res.* 1843, 2012–2026. <https://doi.org/10.1016/j.bbamcr.2014.05.012>.
- Carrella, S., Indrieri, A., Franco, B., Banfi, S., 2020. Mutation-independent therapies for retinal diseases: focus on gene-based approaches. *Front. Neurosci.* 14 <https://doi.org/10.3389/fnins.2020.588234>.
- Casado, M., Sierra, C., Batllori, M., Artuch, R., Ormazabal, A., 2018. A targeted metabolomic procedure for amino acid analysis in different biological specimens by ultra-high-performance liquid chromatography-tandem mass spectrometry. *Metabolomics* 14 (6), 76. <https://doi.org/10.1007/s11306-018-1374-4>.
- Chen, Y., Sawada, O., Kohno, H., Le, Y.Z., Subauste, C., Maeda, T., Maeda, A., 2013. Autophagy protects the retina from light-induced degeneration. *J. Biol. Chem.* 288, 7506–7518. <https://doi.org/10.1074/jbc.M112.439935>.
- Cherubini, M., Puigdel·l·lvoll, M., Alberch, J., Ginés, S., 2015. Cdk5-mediated mitochondrial fission: a key player in dopaminergic toxicity in Huntington's disease. *Biochim. Biophys. Acta Mol. basis Dis.* 1852, 2145–2160. <https://doi.org/10.1016/j.bbadis.2015.06.025>.
- Domenech, E.B., Andres, R., Lopez-Iniesta, Jose, Mirra, S., Arroyo, R.G., Milla, S., Sava, F., Andilla, J., Alvarez, P.L., De La Villa, P., Duarte, R.G., Marfany, G., 2020. A New cerkl mouse model generated by crispr-cas9 shows progressive retinal degeneration and altered morphological and electrophysiological phenotype. *Investig. Ophthalmol. Vis. Sci.* 61 <https://doi.org/10.1167/IOVS.61.8.14>.
- Eells, J.T., 2019. Mitochondrial dysfunction in the aging retina. *Biology (Basel)*. 8 <https://doi.org/10.3390/biology8020031>.
- Esteban-Martínez, L., Doménech, E., Boya, P., Salazar-Roa, M., Malumbres, M., 2015. Mitophagy in mitosis: more than a myth. *Autophagy*. 11, 2379–2380. <https://doi.org/10.1080/15548627.2015.1108509>.
- Fathinajafabadi, A., Pérez-Jiménez, E., Riera, M., Knecht, E., González-Duarte, R., 2014. CERKL, a retinal disease gene, encodes an mRNA-binding protein that localizes in compact and untranslated mRNPs associated with microtubules. *PLoS One*. <https://doi.org/10.1371/journal.pone.0087898>.
- Garanto, A., Riera, M., Pomares, E., Permanyer, J., de Castro-Mir, M., Sava, F., Abril, J.F., Marfany, G., González-Duarte, R., 2011. High transcriptional complexity of the retinitis pigmentosa CERKL gene in human and mouse. *Investig. Ophthalmol. Vis. Sci.* 52, 5202–5214. <https://doi.org/10.1167/IOVS.10.7101>.
- Garanto, A., Vicente-Tejedor, J., Riera, M., De la Villa, P., González-Duarte, R., Blanco, R., Marfany, G., 2012. Targeted knockdown of Cerkl, a retinal dystrophy gene, causes mild affection of the retinal ganglion cell layer. *Biochim. Biophys. Acta Mol. basis Dis.* 1822, 1258–1269. <https://doi.org/10.1016/j.bbadis.2012.04.004>.
- Garanto, A., Mandal, N.A., Egidio-Gabás, M., Marfany, G., Fabriás, G., Anderson, R.E., Casas, J., González-Duarte, R., 2013. Specific sphingolipid content decrease in Cerkl knockdown mouse retinas. *Exp. Eye Res.* <https://doi.org/10.1016/j.exer.2013.03.003>.
- Gatica, D., Lahiri, V., Klionsky, D.J., 2018. Cargo recognition and degradation by selective autophagy. *Nat. Cell Biol.* 20, 233–242. <https://doi.org/10.1038/s41556-018-0037-z>.
- Gatlift, J., Campanella, M., 2015. TSPO is a REDOX regulator of cell mitophagy. *Biochem. Soc. Trans.* 43, 543–552. <https://doi.org/10.1042/BST20150037>.
- Hu, X., Lu, Z., Yu, S., Reilly, J., Liu, F., Jia, D., Qin, Y., Han, S., Liu, X., Qu, Z., Lv, Y., Li, J., Huang, Y., Jiang, T., Jia, H., Wang, Q., Liu, J., Shu, X., Tang, Z., Liu, M., 2019. CERKL regulates autophagy via the NAD-dependent deacetylase SIRT1. *Autophagy*. 15, 453–465. <https://doi.org/10.1080/15548627.2018.1520548>.
- Huang, D.W., Sherman, B.T., Lempicki, R.A., 2009. Systematic and integrative analysis of large gene lists using DAVID bioinformatics resources. *Nat. Protoc.* 4, 44–57. <https://doi.org/10.1038/nprot.2008.211>.
- Inagaki, Y., Mitsutake, S., Igarashi, Y., 2006. Identification of a nuclear localization signal in the retinitis pigmentosa-mutated RP26 protein, ceramide kinase-like protein. *Biochem. Biophys. Res. Commun.* 343, 982–987. <https://doi.org/10.1016/j.bbrc.2006.03.056>.
- Jiang, D., Xiong, G., Feng, H., Zhang, Z., Chen, P., Yan, B., Chen, L., Gandhervin, K., Ma, C., Li, C., Han, S., Zhang, Y., Liao, C., Lee, T.L., Tse, H.F., Fu, Q.L., Chiu, K., Lian, Q., 2019. Donation of mitochondria by iPSC-derived mesenchymal stem cells protects retinal ganglion cells against mitochondrial complex I defect-induced degeneration. *Theranostics*. 9, 2395–2410. <https://doi.org/10.7150/thno.29422>.
- Khacho, M., Slack, R.S., 2018. Mitochondrial dynamics in the regulation of neurogenesis: from development to the adult brain. *Dev. Dyn.* 247, 47–53. <https://doi.org/10.1002/dvdy.24538>.
- Kim, S., Kim, N., Park, S., Jeon, Y., Lee, J., Yoo, S.J., Lee, J.W., Moon, C., Yu, S.W., Kim, E.K., 2020. Tanycytic TSPO inhibition induces lipophagy to regulate lipid metabolism and improve energy balance. *Autophagy*. 16, 1200–1220. <https://doi.org/10.1080/15548627.2019.1659616>.
- Kooragayala, K., Gotoh, N., Cogliati, T., Nellissery, J., Kaden, T.R., French, S., Balaban, R., Li, W., Covician, R., Swaroop, A., 2015. Quantification of oxygen consumption in retina ex vivo demonstrates limited reserve capacity of photoreceptor mitochondria. *Investig. Ophthalmol. Vis. Sci.* 56, 8428–8436. <https://doi.org/10.1167/IOVS.15-17901>.
- Li, C., Wang, L., Zhang, J., Huang, M., Wong, F., Liu, X., Liu, F., Cui, X., Yang, G., Chen, J., Liu, Y., Wang, J., Liao, S., Gao, M., Hu, X., Shu, X., Wang, Q., Yin, Z., Tang, Z., Liu, M., 2014. CERKL interacts with mitochondrial TRX2 and protects retinal cells from oxidative stress-induced apoptosis. *Biochim. Biophys. Acta Mol. basis Dis.* <https://doi.org/10.1016/j.bbadis.2014.04.009>.
- Love, M.I., Huber, W., Anders, S., 2014. Moderated estimation of fold change and dispersion for RNA-seq data with DESeq2. *Genome Biol.* 15 <https://doi.org/10.1186/s13059-014-0550-8>.
- Lu, T., Zhu, Z., Wu, J., She, H., Han, R., Xu, H., Qin, Z.H., 2019. DRAM1 regulates autophagy and cell proliferation via inhibition of the phosphoinositide 3-kinase-Akt-mTOR-ribosomal protein S6 pathway. *Cell Commun. Signal.* 17 <https://doi.org/10.1186/s12964-019-0341-7>.
- Mandal, A., Drerup, C.M., 2019. Axonal transport and mitochondrial function in neurons. *Front. Cell. Neurosci.* 13 <https://doi.org/10.3389/fncel.2019.00373>.
- McWilliams, T.G., Prescott, A.R., Villarejo-Zori, B., Ball, G., Boya, P., Ganley, I.G., 2019. A comparative map of macroautophagy and mitophagy in the vertebrate eye. *Autophagy*. 15, 1296–1308. <https://doi.org/10.1080/15548627.2019.1580509>.
- Mirra, S., Marfany, G., 2019. Mitochondrial gymnastics in retinal cells: a resilience mechanism against oxidative stress and neurodegeneration. In: *Adv. Exp. Med. Biol.* Springer, pp. 513–517. [https://doi.org/10.1007/978-3-030-27378-1\\_84](https://doi.org/10.1007/978-3-030-27378-1_84).
- Mirra, S., Ulloa, F., Gutierrez-Vallejo, I., Martí, E., Soriano, E., 2016. Function of Armcx3 and Armc10/SVH genes in the regulation of progenitor proliferation and neural differentiation in the chicken spinal cord. *Front. Cell. Neurosci.* 10 <https://doi.org/10.3389/fncel.2016.00047>.
- Mizushima, N., Levine, B., 2020. Autophagy in human diseases. *N. Engl. J. Med.* 383, 1564–1576. <https://doi.org/10.1056/nejma2022774>.
- Morsch, A.L.B.C., Wisniewski, E., Luciano, T.F., Comin, V.H., de Silveira, G.B., de Marques, S.O., Thirupathi, A., Lock, P.C. Silveira, De Souza, C.T., 2019. Cigarette smoke exposure induces ROS-mediated autophagy by regulating sestrin, AMPK, and mTOR level in mice. *Redox Rep.* 24, 27–33. <https://doi.org/10.1080/13510002.2019.1601448>.
- Nagata, M., Arakawa, S., Yamaguchi, H., Torii, S., Endo, H., Tsujioka, M., Honda, S., Nishida, Y., Konishi, A., Shimizu, S., 2018. Dram1 regulates DNA damage-induced alternative autophagy. *Cell Stress*. 2, 55–65. <https://doi.org/10.15698/cst2018.03.127>.
- Narayan, D.S., Chidlow, G., Wood, J.P.M., Casson, R.J., 2017. Glucose metabolism in mammalian photoreceptor inner and outer segments. *Clin. Exp. Ophthalmol.* 45, 730–741. <https://doi.org/10.1111/ceo.12952>.
- Nevet, M.J., Vekslin, S., Dizhoor, A.M., Olshevskaya, E.V., Tidhar, R., Futerman, A.H., Ben-Yosef, T., 2012. Ceramide kinase-like (CERKL) interacts with neuronal calcium sensor proteins in the retina in a cation-dependent manner. *Investig. Ophthalmol. Vis. Sci.* 53, 4565–4574. <https://doi.org/10.1167/IOVS.12-9770>.
- Parmigiani, A., Nourbakhsh, A., Ding, B., Wang, W., Kim, Y.C., Akopiants, K., Guan, K.L., Karin, M., Budanov, A.V., 2014. Sestrins inhibit mTORC1 kinase activation through the GATOR complex. *Cell Rep.* 9, 1281–1291. <https://doi.org/10.1016/j.celrep.2014.10.019>.
- Perron, N.R., Beeson, C., Rohrer, B., 2013. Early alterations in mitochondrial reserve capacity: a means to predict subsequent photoreceptor cell death. *J. Bioenerg. Biomembr.* 45, 101–109. <https://doi.org/10.1007/s10863-012-9477-5>.
- Punzo, C., Kornacker, K., Cepko, C.L., 2009. Stimulation of the insulin/mTOR pathway delays cone death in a mouse model of retinitis pigmentosa. *Nat. Neurosci.* 12, 44–52. <https://doi.org/10.1038/nn.2234>.
- Riera, M., Burguera, D., Garcia-Fernández, J., González-Duarte, R., 2013. CERKL knockdown causes retinal degeneration in Zebrafish. *PLoS One*. <https://doi.org/10.1371/journal.pone.0064048>.
- Rosignol, I., Villarejo-Zori, B., Teresak, P., Sierra-Filardi, E., Pereiro, X., Rodríguez-Muela, N., Vecino, E., Vieira, H.L.A., Bell, K., Boya, P., 2020. The mito-QC reporter for quantitative mitophagy assessment in primary retinal ganglion cells and experimental glaucoma models. *Int. J. Mol. Sci.* 21 <https://doi.org/10.3390/ijms21051882>.
- Salcher, S., Hermann, M., Kiechl-Kohlendorfer, U., Ausserlechner, M.J., Obexer, P., 2017. C10orf10/DEPP-mediated ROS accumulation is a critical modulator of FOXO3-induced autophagy. *Mol. Cancer* 16. <https://doi.org/10.1186/s12943-017-0661-4>.
- Scaini, G., Barichello, T., Fries, G.R., Kennon, E.A., Andrews, T., Nix, B.R., Zunta-Soares, G., Valvassori, S.S., Soares, J.C., Quevedo, J., 2019. TSPO upregulation in bipolar disorder and concomitant downregulation of mitophagic proteins and NLRP3 inflammasome activation. *Neuropsychopharmacology*. 44, 1291–1299. <https://doi.org/10.1038/s41386-018-0293-4>.
- Stepp, M.W., Folz, R.J., Yu, J., Zelko, I.N., 2014. The c10orf10 gene product is a new link between oxidative stress and autophagy. *Biochim. Biophys. Acta, Mol. Cell Res.* 1843, 1076–1088. <https://doi.org/10.1016/j.bbamcr.2014.02.003>.
- Tretter, L., Patocs, A., Chinopoulos, C., 2016. Succinate, an intermediate in metabolism, signal transduction, ROS, hypoxia, and tumorigenesis. *Biochim. Biophys. Acta Bioenerg.* 1857, 1086–1101. <https://doi.org/10.1016/j.bbabi.2016.03.012>.
- Tuson, M., Marfany, G., González-Duarte, R., 2004. Mutation of CERKL, a novel human ceramide kinase gene, causes autosomal recessive retinitis pigmentosa (RP26). *Am. J. Hum. Genet.* 74, 128–138. <https://doi.org/10.1086/381055>.
- Tuson, M., Garanto, A., González-Duarte, R., Marfany, G., 2009. Overexpression of CERKL, a gene responsible for retinitis pigmentosa in humans, protects cells from apoptosis induced by oxidative stress. *Mol. Vis.* 15, 168–180.
- Twig, G., Elorza, A., Molina, A.J.A., Mohamed, H., Wikstrom, J.D., Walzer, G., Stiles, L., Haigh, S.E., Katz, S., Las, G., Alroy, J., Wu, M., Py, B.F., Yuan, J., Deeney, J.T., Corkey, B.E., Shirihai, O.S., 2008. Fission and selective fusion govern mitochondrial

- segregation and elimination by autophagy. *EMBO J.* 27, 433–446. <https://doi.org/10.1038/sj.emboj.7601963>.
- Van Noolen, L., Acquaviva-Bourdain, C., Dessein, A.F., Minet-Quinard, R., Nowoczyn, M., Garnotel, R., Corne, C., 2020. Recommendations for urinary organic acids analysis. *Ann. Biol. Clin. (Paris)*. 78, 547–554. <https://doi.org/10.1684/ABC.2020.1583>.
- Villarroya, J., Diaz-Delfin, J., Hyink, D., Domingo, P., Giralt, M., Klotman, P.E., Villarroya, F., 2010. HIV type-1 transgene expression in mice alters adipose tissue and adipokine levels: towards a rodent model of HIV type-1 lipodystrophy. *Antivir. Ther.* 15, 1021–1028. <https://doi.org/10.3851/IMP1669>.
- Wu, X., Qin, Y., Zhu, X., Liu, D., Chen, F., Xu, S., Zheng, D., Zhou, Y., Luo, J., 2018. Increased expression of DRAM1 confers myocardial protection against ischemia via restoring autophagy flux. *J. Mol. Cell. Cardiol.* 124, 70–82. <https://doi.org/10.1016/j.yjmcc.2018.08.018>.
- Yang, Y., Klionsky, D.J., 2020. Autophagy and disease: unanswered questions. *Cell Death Differ.* 27, 858–871. <https://doi.org/10.1038/s41418-019-0480-9>.
- Yang, W., Xiong, G., Lin, B., 2020. Cyclooxygenase-1 mediates neuroinflammation and neurotoxicity in a mouse model of retinitis pigmentosa. *J. Neuroinflammation* 17. <https://doi.org/10.1186/s12974-020-01993-0>.
- Yoon, J.H., Her, S., Kim, M., Jang, I.S., Park, J., 2012. The expression of damage-regulated autophagy modulator 2 (DRAM2) contributes to autophagy induction. *Mol. Biol. Rep.* 39, 1087–1093. <https://doi.org/10.1007/s11033-011-0835-x>.
- Zaninello, M., Palikaras, K., Naon, D., Iwata, K., Herkenne, S., Quintana-Cabrera, R., Semenzato, M., Grespi, F., Ross-Cisneros, F.N., Carelli, V., Sadun, A.A., Tavernarakis, N., Scorrano, L., 2020. Inhibition of autophagy curtails visual loss in a model of autosomal dominant optic atrophy. *Nat. Commun.* 11 <https://doi.org/10.1038/s41467-020-17821-1>.
- Zemirli, N., Morel, E., Molino, D., 2018. Mitochondrial dynamics in basal and stressful conditions. *Int. J. Mol. Sci.* 19 <https://doi.org/10.3390/ijms19020564>.
- Zhang, Z., Yan, B., Gao, F., Li, Q., Meng, X., Chen, P., Zhou, L., Deng, W., Li, C., Xu, W., Han, S., Feng, H., Li, Y., Chen, J., Yin, Z., Liao, C., Tse, H.F., Xu, A., Lian, Q., 2020. PSCs reveal PUFA-provoked mitochondrial stress as a central node potentiating RPE degeneration in Bietti's crystalline dystrophy. *Mol. Ther.* 28, 2642–2661. <https://doi.org/10.1016/j.ymthe.2020.07.024>.